AMERICAN SOCIETY FOR MICROBIOLOGY | mBio®

RESEARCH ARTICLE

Penicillin-Binding Protein 1 (PBP1) of *Staphylococcus aureus* Has Multiple Essential Functions in Cell Division

Katarzyna Wacnik,[a,b] Vincenzo A. Rao,[c] Xinyue Chen,[b,d] Lucia Lafage,[a,b] Manuel Pazos,[e] Simon Booth,[c] Waldemar Vollmer,[e] Jamie K. Hobbs,[b,d] Richard J. Lewis,[c*] Simon J. Foster[a,b]

[a]School of Biosciences, University of Sheffield, Sheffield, United Kingdom
[b]The Florey Institute for Host-Pathogen Interactions, University of Sheffield, Sheffield, United Kingdom
[c]Biosciences Institute, Newcastle University, Newcastle upon Tyne, United Kingdom
[d]Department of Physics and Astronomy, University of Sheffield, Sheffield, United Kingdom
[e]Centre for Bacterial Cell Biology, Bioscience Institute, Newcastle University, Newcastle upon Tyne, United Kingdom

ABSTRACT Bacterial cell division is a complex process requiring the coordination of multiple components to allow the appropriate spatial and temporal control of septum formation and cell scission. Peptidoglycan (PG) is the major structural component of the septum, and our recent studies in the human pathogen *Staphylococcus aureus* have revealed a complex, multistage PG architecture that develops during septation. Penicillin-binding proteins (PBPs) are essential for the final steps of PG biosynthesis; their transpeptidase activity links the peptide side chains of nascent glycan strands. PBP1 is required for cell division in *S. aureus*, and here, we demonstrate that it has multiple essential functions associated with its enzymatic activity and as a regulator of division. Loss of PBP1, or just its C-terminal PASTA domains, results in cessation of division at the point of septal plate formation. The PASTA domains can bind PG and thereby potentially coordinate the cell division process. The transpeptidase activity of PBP1 is also essential, but its loss leads to a strikingly different phenotype of thickened and aberrant septa, which is phenocopied by the morphological effects of adding the PBP1-specific β-lactam, meropenem. Together, these results lead to a model for septal PG synthesis where PBP1 enzyme activity is required for the characteristic architecture of the septum and PBP1 protein molecules enable the formation of the septal plate.

IMPORTANCE Bacterial cell wall peptidoglycan is essential, and its synthesis is the target of clinically important antibiotics such as β-lactams. β-lactams target penicillin-binding proteins (PBPs) that assemble new peptidoglycan from its building blocks. The human pathogen *Staphylococcus aureus* only has two essential PBPs that can carry out all the functions necessary for growth and division. In the absence of the confounding antibiotic resistance-associated PBP PBP2A, PBP1 is required for cell division, and here, we have found that it has several essential functions, both as an enzyme and as a coordinator by binding to cell division proteins and to its peptidoglycan product, via its PASTA domains. This has led to a new model for cell division with PBP1 responsible for the synthesis of the characteristic architectural features of the septum.

KEYWORDS *Staphylococcus aureus*, cell division, penicillin-binding proteins, peptidoglycan

Peptidoglycan (PG) is the major structural component of the bacterial cell wall and is essential for maintaining cell shape, integrity, and survival (1–3). The final stages of assembly of this large polymeric molecule are mediated by penicillin-binding proteins (PBPs), key PG synthases that, through their transglycosylase (TG) and

Editor Gerard D. Wright, McMaster University

Address correspondence to Simon J. Foster, s.foster@sheffield.ac.uk.
*Present address: Richard J. Lewis, The Royal Society for the Protection of Birds, Sandy, Bedfordshire, United Kingdom.
The authors declare no conflict of interest.
Received 11 March 2022
Accepted 13 May 2022
Published 15 June 2022

transpeptidase (TP) activities, polymerize glycan chains and cross-link them into a mesh-like hydrogel (4, 5). Since the cell wall is essential for maintaining bacterial life, PBPs and PG synthesis are a target of some of the most important antibiotics, β-lactams (penicillins) and glycopeptides (vancomycin) (6, 7). The major human pathogen *Staphylococcus aureus* has a minimalist PBP system, as it encodes only four PBPs, PBP1 to PBP4 (8). Only PBP1 (class B PBP with only TP activity, bPBP) and PBP2 (class A bifunctional PBP with both TG and TP activities, aPBP) are essential and sufficient for septal and peripheral PG synthesis in *S. aureus* (8, 9). PBP2 is the major PG synthase of *S. aureus*, and the septum formation activity of PBP2 is mediated by its substrate, lipid II (10). Although PBP2 is essential, loss of its TP activity can be compensated for by a horizontally acquired class B PBP2A in methicillin-resistant *S. aureus* (MRSA) (11). PBP2A, however, cannot replace PBP1, whose loss is detrimental to the viability of *S. aureus* (12). PBP1 and PBP3 (bPBP) form cognate pairs with the monofunctional TGs, FtsW and RodA, belonging to the SEDS (shape, elongation, division, and sporulation) family (13) to facilitate septum formation (PBP1-FtsW) and to maintain the prolate cell shape (PBP3-RodA) of *S. aureus*, respectively (14). Activation of the transglycosylase activity of FtsW requires complex formation with PBP1 (15). PBP4 is a class C PBP with D,D-carboxypeptidase activity (cPBP) and has a TP activity that contributes to the high-level cross-linking of PG and MRSA resistance to β-lactams (16, 17).

The cell wall of Gram-positive bacteria is decorated with wall teichoic acid (WTA) glycopolymers (18). WTA regulates cell shape, ion homeostasis, autolytic enzymes, growth, and division (19). In *S. aureus*, WTA plays a crucial role in virulence, MRSA resistance to β-lactam antibiotics, PBP4 localization at the septum, and PG cross-linking (20–23).

Although *S. aureus* PBPs have been studied over many years, the specific roles of PBP1 in cell division, PG synthesis, and architecture are not well understood. Previous studies have shown that while PBP1 is essential, its TP activity is not, implying another role (12, 14). However, this work was performed in an MRSA background that contains PBP2A, encoded by *mecA*, which is non-native to *S. aureus* (24). While PBP2A cannot replace PBP1, how these proteins interact is unknown. We have recently shown that the presence of *mecA* has a profound effect on cellular physiology (25). Thus, it is important to understand individual and combined roles of *S. aureus* PBPs in both the presence and absence of the exogenous PBP2A, as the vast majority of *S. aureus* infections are caused by methicillin-sensitive strains.

RESULTS

***S. aureus* PBP1 PASTA domains are essential for growth and PBP1 functionality.** PBP1 has a short cytoplasmic fragment, a membrane-spanning sequence, an exocytoplasmic N-terminal pedestal domain, and a C-terminal region consisting of the TP domain and two PASTA domains (for penicillin-binding protein and serine/threonine kinase-associated domain) (26, 27). We created a set of conditional mutants of *pbp1* to investigate the role of PBP1 in cell division and PG synthesis. An ectopic copy of *pbp1* under the control of the P*spac* promoter (P_{spac}-*pbp1*) was placed at the lipase locus (*geh*::P_{spac}-*pbp1*) of *S. aureus* SH1000, and a series of changes were made in this genetic background at the native *pbp1* locus: (i) an in-frame deletion of *pbp1* (Δ*pbp1*), (ii) a deletion of the region encoding the two PASTA domains ($pbp1_{\Delta PASTA}$), and (iii) the substitution of the catalytic Ser314 to Ala in the TP domain (*pbp1**) (Fig. 1A and B). We examined the essentiality of PBP1, the PASTA domains, and the active TP domain with these mutants. Depletion of PBP1 via IPTG (isopropyl-β-D-thiogalactopyranoside) removal (Fig. 1C and Fig. S1A and B) resulted in cell death, confirming the essentiality of PBP1 (Fig. 1C and D and Fig. S1C and D). Deletion of the PASTA domains also led to growth inhibition and more than 99% cell death within 4 h (Fig. 1D and Fig. S1C and D). Importantly, this phenotype was not associated with $PBP1_{\Delta PASTA}$ instability (Fig. 1C and Fig. S1A) or loss of its ability to bind its substrate analogue BocillinFL (Fig. S1B). In contrast, deletion of the PASTA domains of *Streptococcus pneumoniae* PBP2x, a PBP1 orthologue, resulted in a complete loss of

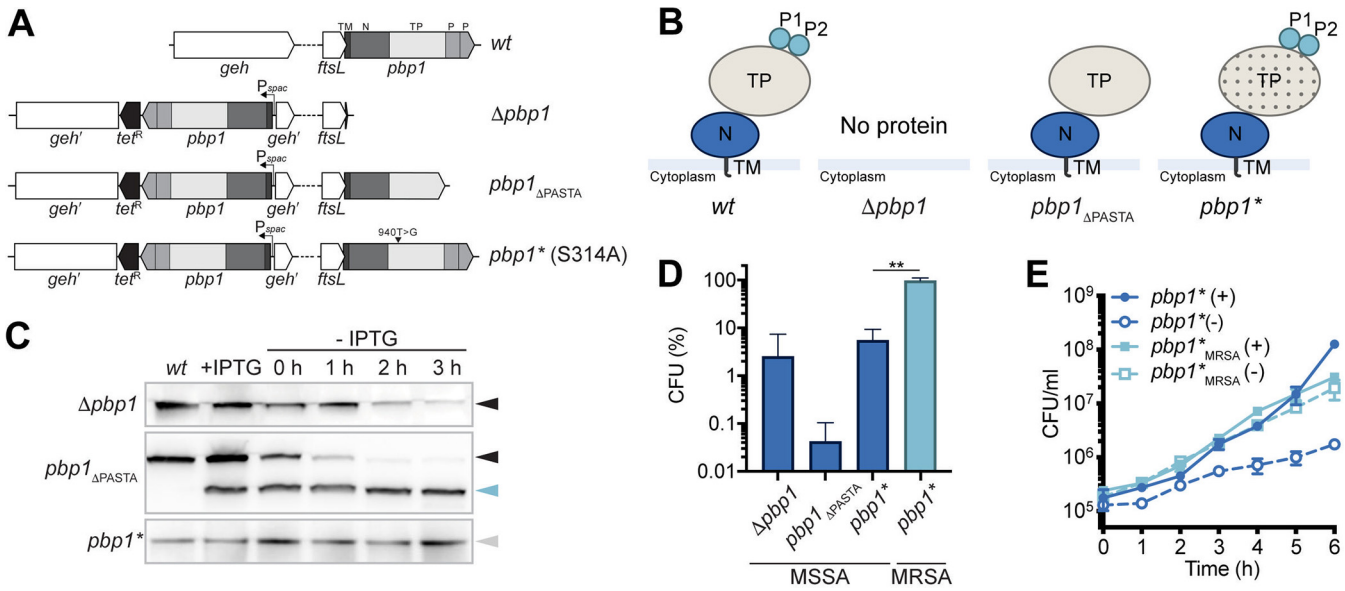

FIG 1 PBP1, its PASTA domains, and transpeptidase activity are essential in MSSA. (A) Schematic representation of genetic constructs used in this study. In *S. aureus* WT (*wt*) the 5′ end of *pbp1* overlaps with the 3′ end of *ftsL*. The *pbp1* gene encodes a protein containing the short cytoplasmic tail, transmembrane helix (TM), N-terminal pedestal domain (N), transpeptidase (TP) domain, and two PASTA domains (P1 and P2). In the mutants, an ectopic copy of *pbp1* is placed under the control of the P*spac* promoter at the lipase (*geh*) locus, whereas the gene in the native *pbp1* locus is either deleted (Δ*pbp1*), has P1 and P2 domains removed ($pbp1_{\Delta PASTA}$), or has a point mutation which results in inactivation of the TP domain (*pbp1**). (B) Schematic representation of the domain architecture of PBP1 in *S. aureus* WT (*wt*) and PBP1 forms produced by Δ*pbp1*, $pbp1_{\Delta PASTA}$, and *pbp1** mutants in the absence of inducer. The TP domain inactivation is shown by dotted shading. (C) Immunoblot showing PBP1 levels in SH1000 *lacI* (*wt*) and in Δ*pbp1*, $pbp1_{\Delta PASTA}$, and *pbp1** grown with IPTG (+IPTG) and for 0, 1, 2, and 3 h without inducer (–IPTG) analyzed using anti-PBP1 antibody. Expected sizes: PBP1 and PBP1* = 83 kDa (black and gray arrowheads, respectively) and $PBP1_{\Delta PASTA}$ = 67 kDa (light blue arrowhead). (D) Plating efficiency of Δ*pbp1*, $pbp1_{\Delta PASTA}$, and *pbp1** (MSSA) cells and MRSA *pbp1** ($pbp1*_{MRSA}$) cells upon inducer removal compared to the control groups grown in the presence of inducer. The *P* value was determined by Mann-Whitney *U* tests. $P = 0.0043$ (**, $P < 0.01$). Data represent the mean ± standard deviation (SD). (E) Growth curves of *pbp1** (MSSA) and MRSA *pbp1**($pbp1*_{MRSA}$) in the presence (+) or absence (–) of IPTG. Data represent the mean ± SD. Error bars that are smaller than the symbols are not shown. Data are representative of three (C and E) and at least four (D) independent experiments.

BocillinFL binding (28). These results indicate that the PASTA domains are essential for *S. aureus* growth and PBP1 functionality but not its stability.

During construction of the *pbp1** mutant we obtained, by serendipity, a $pbp1_{STOP}$ mutant in which a single-nucleotide polymorphism (SNP) in the codon for Glu292 resulted in its replacement with a premature stop codon and the truncation of the entire TP and PASTAs region of PBP1 (Fig. S1E and F). However, immunoblot analysis using anti-PBP1 sera could not confirm the presence of the $PBP1_{STOP}$ protein in the $pbp1_{STOP}$ mutant (Fig. S1G), suggesting that stability of the N-terminal domain of PBP1 is dependent on its C terminus but not the PASTA domains. Although inactivation of PBP1 TP activity (PBP1*) did not affect protein stability (Fig. 1C), it did remove the ability of PBP1 to bind BocillinFL (Fig. S1B). The loss of PBP1 TP activity resulted in severely compromised growth on solid medium (Fig. 1D and Fig. S1C) and reduced cellular viability in liquid culture (Fig. 1E and Fig. S1D). Thus, the TP activity of PBP1 is required for growth in the SH1000 background. Inactivation of the PBP1 TP activity was previously reported not to affect growth in the COL strain background (14). The differences in the necessity for the PBP1 TP activity could result from COL being MRSA, whereas SH1000 is a methicillin-sensitive *S. aureus* (MSSA) strain.

PBP1 TP activity is crucial in MSSA but not in MRSA. We have recently developed a set of defined strains where high-level β-lactam resistance of MRSA is mediated by *mecA* encoding PBP2A and a mutation in either *rpoB* or *rpoC* (25). This combination of genetic alterations ($mecA^+$ *rpoB*) is present in COL (25). To test if the apparent disparity in PBP1's role is associated with MRSA, we developed a high-level resistant mutant of *pbp1** in the well-characterized *S. aureus* SH1000 by adding the *mecA* $rpoB^{H929Q}$ to the MSSA *pbp1** mutant, resulting in $SH1000_{MRSA}$ *pbp1** (Fig. S2A). Inactivating PBP1 TP did not affect the ability of $SH1000_{MRSA}$ *pbp1** to grow in the absence of IPTG, whereas *pbp1* depletion led to growth inhibition in the isogenic Δ*pbp1* MSSA and MRSA strains

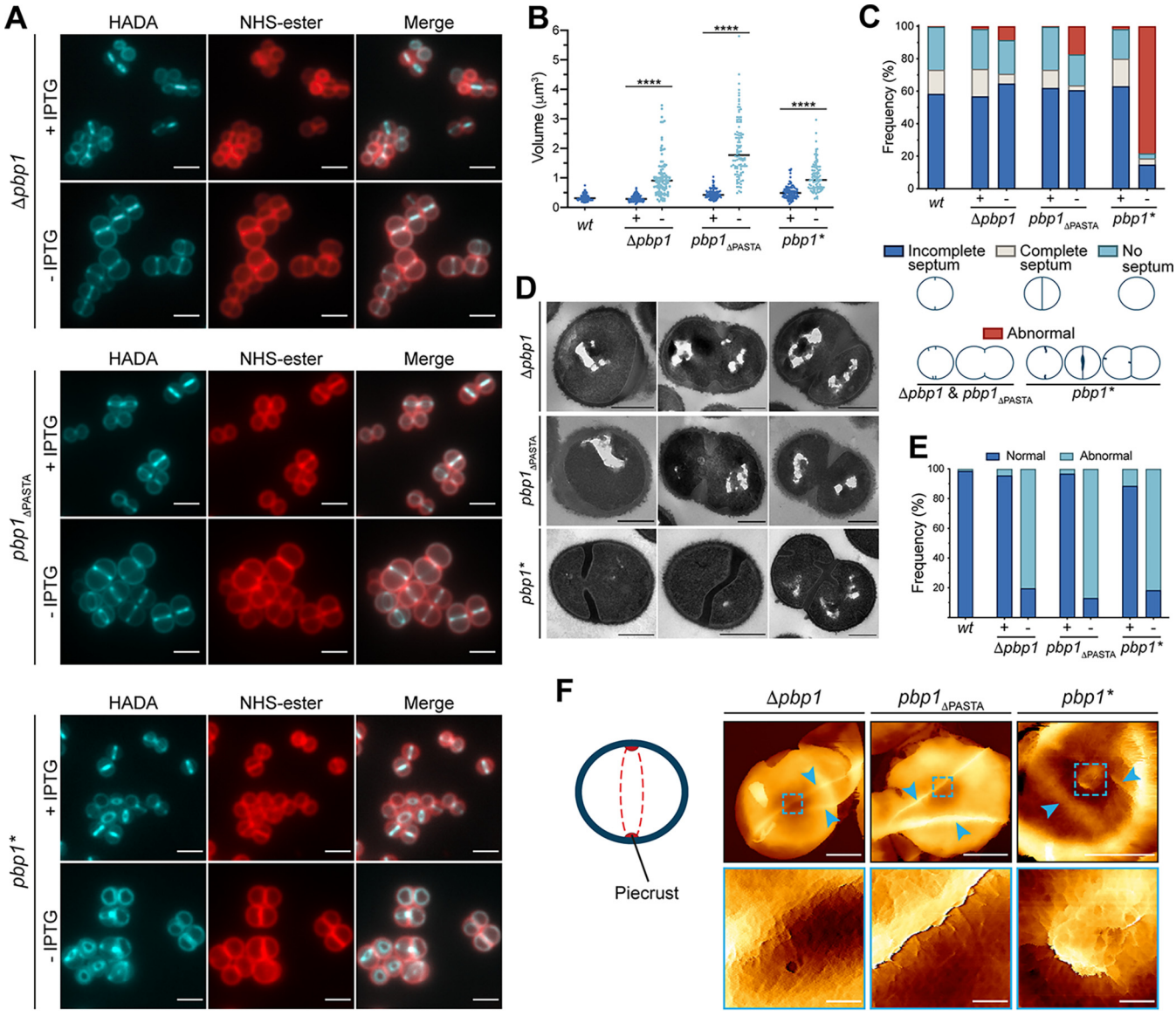

FIG 2 Role of PBP1 in cell division and PG synthesis in *S. aureus*. (A) Δ*pbp1*, *pbp1*$_{\Delta PASTA}$, and *pbp1** grown with or without IPTG for 2 h, incubated with HADA for 5 min to show nascent PG, and counterlabeled with NHS-ester Alexa Fluor 555 to image the cell wall. Images are average intensity projections of z stacks. Scale bars = 2 μm. (B) Cell volumes of SH1000 *lacI* (*wt*) and Δ*pbp1*, *pbp1*$_{\Delta PASTA}$, and *pbp1** grown with (+) or without (–) IPTG for 2 h as measured by fluorescence microscopy after NHS-ester Alexa Fluor 555 labeling. Each dot represents a single cell. The median of each distribution is indicated by a black line. The *P* value was determined by Mann-Whitney *U* tests (****, $P < 0.0001$). From left to right, $P = 3.033e\text{-}033$, $4.670e\text{-}049$, and $2.206e\text{-}022$. The number of cells analyzed for each mutant and condition was $n \geq 100$. (C) Quantification of cellular phenotypes for SH1000 *lacI* (*wt*) and Δ*pbp1*, *pbp1*$_{\Delta PASTA}$, and *pbp1** based on HADA incorporation (panel A) after incubation with (+) or without (–) IPTG for 2 h. From left to right, $n = 370, 427, 332, 314, 364, 512$, and 331. (D) TEM of Δ*pbp1*, *pbp1*$_{\Delta PASTA}$, and *pbp1** grown for 2 h in the absence of inducer. Scale bars = 500 nm. (E) Quantification of cellular phenotypes based on TEM data of SH1000 *lacI* (*wt*) and Δ*pbp1*, *pbp1*$_{\Delta PASTA}$, and *pbp1** grown for 2 h in the presence (+) or absence (–) of IPTG. Examples of cells classified as normal (blue) are shown in Fig. S4B. Cells with abnormal phenotypes (light blue) are shown in panel D and Fig. S4C. From left to right, $n = 304, 391, 329, 314, 377, 263$, and 302. (F) AFM topographic images of internal surface of purified sacculi from Δ*pbp1*, *pbp1*$_{\Delta PASTA}$, and *pbp1** grown in the absence of inducer for 2 h. (Left) Diagram of the inside of the cell before septal plate formation and (right) AFM images of sacculi (top images, scale bars = 500 nm, data scales [z]: 450, 300, and 100 nm from left to right, respectively) and higher magnification images (bottom images, scale bars = 50 nm, data scales [z]: 70, 100, and 50 nm from left to right, respectively) scanned within the boxed areas from the top images. The arrowheads indicate abnormal piecrusts. The boxed areas show details of piecrust features in Δ*pbp1* and *pbp1*$_{\Delta PASTA}$ and material agglomeration in *pbp1**. Data are representative of two (D to F) and (A to C) three independent experiments.

(Fig. 1D and E and Fig. S2B to D). Thus, the fundamental role of PBP1 in growth and division can only be studied in an MSSA background, as otherwise, the role of PBP1 can be confounded by the presence of the MRSA resistance apparatus.

PBP1 PASTA domains are required for septum progression. PG synthesis still occurred in Δ*pbp1*, *pbp1*$_{\Delta PASTA}$, and *pbp1** in the absence of IPTG, despite cell growth

inhibition, as measured by the incorporation of the fluorescent D-amino acid derivative HADA (Fig. 2A). This was not a consequence of the nonsynthesis, exchange reaction carried out by PBP4, as it occurred in *pbp4* as well as with the dipeptide ADA-DA (9, 29) (Fig. S3). All variants increased in cell volume upon depletion of *pbp1*, whereas $pbp1_{\Delta PASTA}$ was enlarged by almost twice as much as Δ*pbp1* and *pbp1** (Fig. 2A and B and Fig. S4A). Despite differences in cell size, both Δ*pbp1* and $pbp1_{\Delta PASTA}$ demonstrated a decrease in the proportion of cells with complete septa compared to the parent (Fig. 2A and C). Transmission electron microscopy (TEM) showed that more than 80% of the population had morphological defects, including cell wall thickening, PG blebs, and misshapen and/or multiple incomplete septa. (Fig. 2D and E and Fig. S4B and C). Such septa had abnormally thick bases and sharply pointed leading edges, suggesting that there is a problem with septal progression after initiation. Atomic force microscopy (AFM) previously revealed that the first step in cell division is the formation of a thick band of PG called the "piecrust" (30). Within this, the septal plate is formed, which has two PG architectures: disordered mesh facing the cell membrane and concentric rings in the septum core (5). Here, lack of PBP1 or the PBP1 PASTA domains led to formation of more than one, and often misplaced, piecrust. These mutations also caused an increase in unfinished septal annuli and alterations in the PG ring architecture (Fig. 2F and Fig. S5A to C, arrowheads), a feature that is revealed immediately after cell scission (5). Thus, depletion of PBP1 did not stop septum initiation, but the loss of the PASTA domains was enough to cause formation of irregular piecrusts, arrest septal plate formation, and lead to an altered septal PG architecture.

PBP1 TP activity is required for the characteristic septal PG architecture. The *pbp1** mutant gave a novel phenotype quite distinct from loss of entire PBP1 or PASTA domains. Inactivation of PBP1 TP activity did not prevent initiation and closing of the septa but, instead, resulted in accumulation of cells with aberrant septa and separation defects in about 80% of the population (Fig. 2A, C, and E). The septa in such cells had a rounded leading edge, were curved and abnormally thick (Fig. 2D and E and Fig. S4B and C), and had agglomerations of mesh-like material close to the septal center in addition to irregular piecrusts as observed by AFM (Fig. 2F and Fig. S5A and B). The intracellular agglomerations are PG, as they stain heavily with HADA and ADA-DA (Fig. 2A and Fig. S3C and F) and could be observed in purified sacculi (Fig. 2F and Fig. S5B). No ring architecture, only mesh-structured PG, could be observed on the surface of the *pbp1** mutant. Importantly, with fluorescence microscopy, the *pbp1* pbp3 pbp4* mutant, in which PBP2 is the only active TP, presented a similar phenotype upon IPTG removal as *pbp1**, exemplified by misshapen septa and agglomerations of PG material marked by HADA (Fig. S4D). Therefore, aberrant septal synthesis and progression occur in the *pbp1** mutant. Associated PG synthesis results from PBP2 transpeptidase activity and potentially the transglycosylase activity of FtsW, acting to produce un-cross-linked glycan strands.

The *pbp1** phenotype occurred specifically because of the loss of the TP activity of this essential enzyme. This phenotype is mirrored by the mode of action of β-lactam antibiotics, which bind to and inhibit the TP activity of PBPs (7). We have recently described the morphological effects of methicillin and oxacillin on *S. aureus*, which result in cell swelling and cessation of septal and peripheral cell wall synthesis (31). Our results suggest that PBP1 TP activity has a role in septal plate formation, and without this, the septum is misshapen. The conditional lethal strains made here allow for functional analysis of the genes concerned. However, phenotypes tend to accumulate on depletion of the wild-type protein over time, confusing the precise roles for individual components. To independently corroborate the role of the TP activity of PBP1, we utilized an approach to directly, and selectively, inhibit its activity. Meropenem (MEM) has a higher affinity for PBP1 than PBP2 (32, 33), and therefore, we hypothesized that its effect on *S. aureus* would match that of *pbp1**. In a MEM-titration, treatment with 1× MIC of MEM was sufficient to lead to cell death and a significant increase in SH1000 wild-type (WT) cell volume after 1 h (Fig. 3A and B and Fig. S6A). More than 70% of

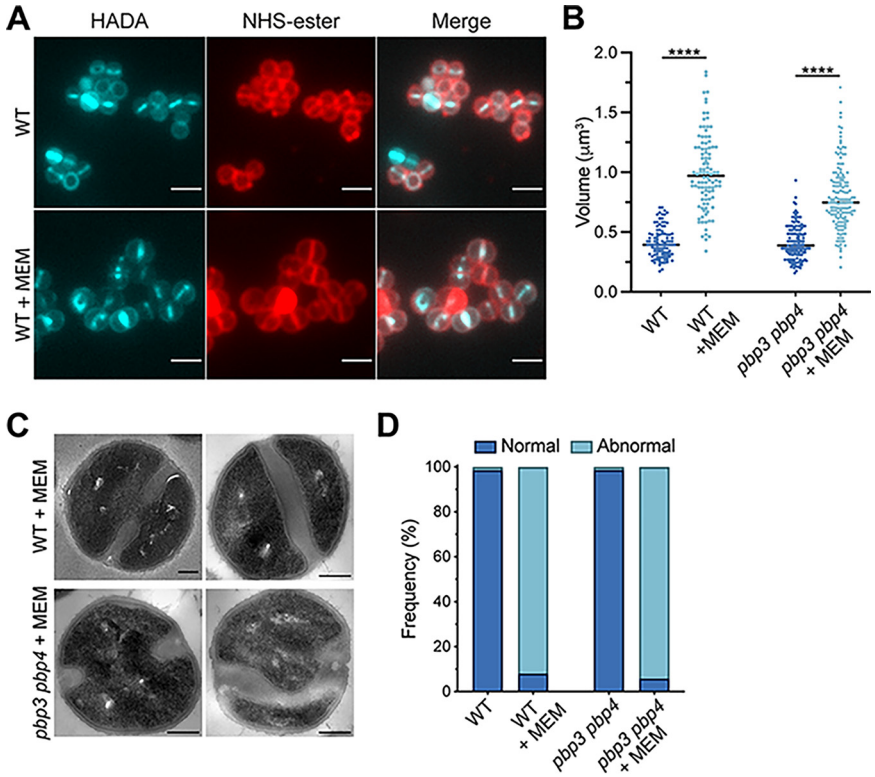

FIG 3 Effect of meropenem (MEM), an antibiotic with high affinity for PBP1, on *S. aureus*. (A) Fluorescence images of SH1000 WT treated with 1× MIC of MEM for 1 h, labeled with HADA for 5 min to show nascent PG, and counterlabeled with NHS-ester Alexa Fluor 555 (cell wall). Images are average intensity projections of z stacks. Scale bars = 2 μm. (B) Cell volumes of SH1000 WT and *pbp3 pbp4* treated with 1× MIC of MEM for 1 h as measured by fluorescence microscopy after NHS-ester Alexa Fluor 555 labeling (panel A). Each dot represents a single cell. The median of each distribution is indicated by a black line. The *P* value was determined by Mann-Whitney *U* tests (****, $P < 0.0001$). From left to right, $P = 1.276e\text{-}042$ and $1.303e\text{-}034$. The number of cells analyzed for each condition was $n \geq 100$. (C) TEM of SH1000 WT and *pbp3 pbp4* treated with 1× MIC of MEM for 1 h. Scale bars = 200 nm. (D) Quantification of phenotypes of SH1000 WT and *pbp3 pbp4* treated with MEM (1× MIC) for 1 h based on TEM data (panel C and Fig. S6E and F). Examples of cells classified as normal (blue) are shown in Fig. S6E and F. Cells with abnormal phenotypes (light blue) are shown in panel C and Fig. S6E and F. From left to right, $n = 343$, 287, 403, and 365. Data are representative of two independent experiments.

MEM-treated cells had growth defects that manifested as aberrantly shaped septa and accumulation of PG as shown by HADA labeling (Fig. 3A, C, and D and Fig. S6C and E), similar to observations made with the *pbp1** mutants (Fig. 2A and C to E and Fig. S3C and F). The MEM phenotype of malformed septa was not linked to PBP3 or PBP4, as it was also observed in the corresponding double mutant (Fig. 3C and D and Fig. S6B, D, and F), which corroborated the role of PBP2 in misshapen septal genesis. The MEM phenotype differed from methicillin treatment, which inhibits both PBP1 and PBP2, as this results in a cessation of PG synthesis and apparent plasmolysis (31).

PASTA domains mediate PBP1 interaction with division-associated components. The morphologies of the Δ*pbp1* and $pbp1_{\Delta PASTA}$ mutants resemble *S. aureus* depleted of DivIB in which EzrA and FtsZ form multiple rings and the synthesis of the cross wall is blocked, despite the normal recruitment of early cell division proteins and piecrust formation (34). EzrA is a marker of early division protein recruitment but also remains until septal completion (9, 35). In the Δ*pbp1 ezrA-gfp* strain, EzrA, which here acts as an early cell division marker, was localized at midcell in the majority of cells and formed additional arcs or rings in 33% of the population (Fig. 4A and D). Multiple EzrA rings were observed in 43% of the $pbp1_{\Delta PASTA}$ *ezrA-gfp* mutant cells (Fig. 4B and D), supporting the requirement for PBP1 PASTA domains for correct selection of the division site and/or

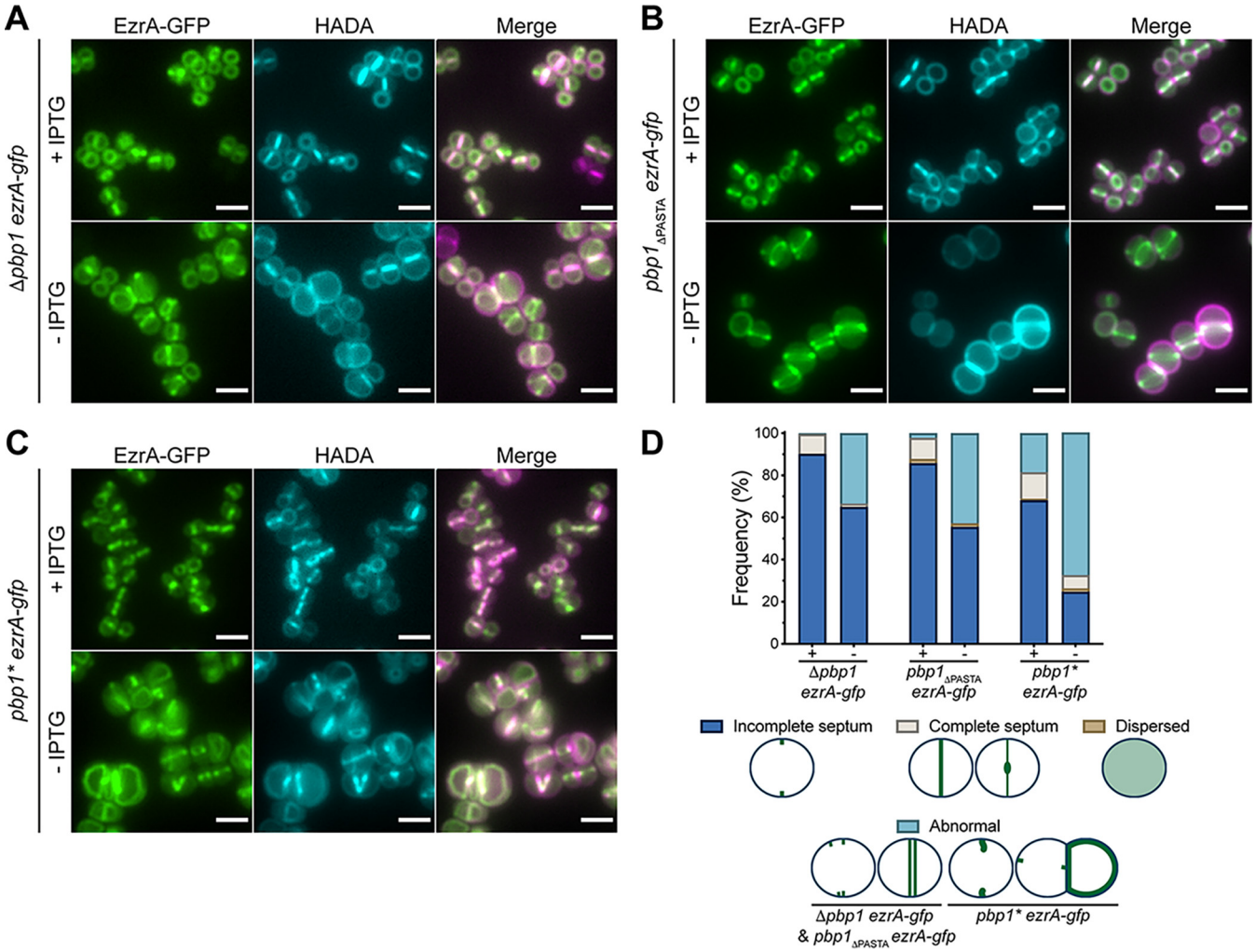

FIG 4 Role of PBP1, PASTA, and TP domains in EzrA localization in *S. aureus*. (A to C) Localization of EzrA-GFP in Δ*pbp1 ezrA-gfp*, *pbp1*$_{\Delta PASTA}$ *ezrA-gfp*, and *pbp1* ezrA-gfp* grown in the presence or absence of IPTG for 2 h and labeled with HADA for 5 min to stain PG. Images are average intensity projections of z stacks. Scale bars = 5 μm. (D) Quantification of EzrA-GFP localizations in Δ*pbp1 ezrA-gfp*, *pbp1*$_{\Delta PASTA}$ *ezrA-gfp*, and *pbp1* ezrA-gfp* grown with or without IPTG. "Abnormal" includes those cells with multiple and/or misplaced EzrA rings. From left to right, n = 395, 499, 481, 438, 360, and 382. Data are representative of two independent experiments.

septal progression. Alternatively, the multiple division rings could result from a lack of the septal progression whereby the unproductive division machinery results in futile additional alternative initiation attempts, suggesting that PASTA domains are involved in the progression from piecrust to septal plate formation. While the number of cells with complete septa (EzrA-GFP visible as a line or focus) decreased by at least 6-fold in Δ*pbp1 ezrA-gfp* and *pbp1*$_{\Delta PASTA}$ *ezrA-gfp*, it only halved in *pbp1* ezrA-gfp* (12.5% to 6.3% of *pbp1* ezrA-gfp* grown with or without IPTG, respectively; Fig. 4C and D), confirming that septum progression, although reduced, still occurred when PBP1 TP was inactive, implying that TP activity is necessary for correct septal architecture during cell division.

PBP1 is important for the septal surface PG ring structure (Fig. 2F and Fig. S5B), where it has been proposed that mature WTA is not present throughout the septum (23, 36). Loss of WTA also results in a proportion of cells with aberrant septa (21), suggesting a potential link with PBP1 function. Loss of *tarO* (leading to a lack of WTA) caused minor cell division defects in SH1000 (Fig. S7A, E, and F). Combining *tarO* with the mutations in *pbp1* exacerbated the observed morphological defects, with the appearance of distinct septal and off-septal PG foci appearing (marked with HADA) in Δ*pbp1 tarO* and *pbp1*$_{\Delta PASTA}$ *tarO* (Fig. S7B to F), demonstrating that both WTA and PBP1 are involved in cell cycle progression in parallel.

As PBP1 PASTA has a role in the regulation of septal plate formation, this may be determined by interacting with other protein components. In order to examine this hypothesis, we performed a bacterial two-hybrid assay, in which PBP1 has previously been found to have apparent, multiple interactions (35). Truncation of the PASTA domains reduced *S. aureus* PBP1 interaction not only with DivIB but also with FtsW, while recognition of other known interacting partners of PBP1 (EzrA, PBP2, and DivIC) were unaffected by the PASTA truncation (Fig. S8A and B), suggesting that these potential, wider interactions involve the N-terminal domain of PBP1.

PBP1 PASTA domains bind peptidoglycan. Impaired interaction with DivIB could be one explanation for why cells depleted of PBP1 PASTA domains initiate irregular piecrusts and septation defects accrue as a consequence. PASTA domains have long been associated with PG binding because of work performed mainly on serine/threonine protein kinases (STPK) (26, 37–39). Very recently, PBP1 PASTA domains have been shown to bind isolated, small fragments of PG (27). Therefore, we assessed whether *S. aureus* PBP1 and its PASTA domains could recognize PG by measuring their affinities for *S. aureus* cell wall PG with or without WTA (±WTA) with a semiquantitative fluorescence-binding assay and *S. aureus* PBP1 derivatives produced in *Escherichia coli* (Fig. 5A and Fig. S8C). Cytochrome *c* (34) was used as a negative control to rule our nonspecific binding (dissociation constant [K_d], 1,126 ± 37 nM [+WTA] and 1,171 ± 363 nM [–WTA]) (Fig. S8D). Both *Sa*PBP1 (K_d, 19 ± 4 nM [+WTA] and 115 ± 21 nM [–WTA]) and its PASTA domains (*Sa*PASTA$_{PBP1}$; K_d, 198 ± 42 nM [+WTA] and 109 ± 23 nM [–WTA]) bound PG (Fig. 5B). Inactive *Sa*PBP1* was still able to bind PG with a preference for PG with WTA present (K_d, 53 ± 8 nM [+WTA] and 227 ± 46 nM [–WTA]; Fig. 5B), similar to active *Sa*PBP1. Although removal of the PASTA domains did not abolish BocillinFL binding (Fig. S8C), it considerably reduced the ability of *Sa*PBP1$_{\Delta PASTA}$ to bind PG, and binding was abolished in the presence of WTA (K_d, >2,000 nM [+WTA] and 440 ± 57 nM [–WTA]; Fig. 5B). In contrast, the PASTA domains (*Sa*PASTA$_{PBP1}$) on their own bind to *S. aureus* PG but are incapable of binding BocillinFL (Fig. 5B and Fig. S8C). These results demonstrate that PBP1 is a PG-binding protein, and the PASTA domains have a dominant role in this interaction. Sequence conservation analysis of PASTA domains revealed the presence of either Arg or Glu residues in classifying a PASTA domain as a PG-binder (40). The PASTA domains of *S. aureus* PBP1 each have proline at the equivalent positions (residues Pro603 and Pro661), and thus PBP1 would be predicted as a non-PG-binder. Our data suggest that the predicted significance of conserved Arg or Glu residues with regard to PG binding is either only relevant to PASTA domains found in STPKs, linear arrangements of tandem PASTA repeats, or is not suitable for proteins with multiple and complex functions like PBPs.

To gain a better understanding of the role of the PASTA domains in *S. aureus* PBP1 (*Sa*PASTA$_{PBP1}$), we determined their structure by X-ray crystallography. Soluble recombinant protein was obtained in high yield from the cytoplasm of *E. coli* cells, and well-ordered crystals were subsequently produced that diffracted to a maximum resolution of 1.78 Å (Table S1). The structure was solved by molecular replacement using the corresponding PASTA domains present in *Sp*PBP2x from PDB entry 5OAU (41), which shares 26% sequence identity with *Sa*PASTA$_{PBP1}$. The asymmetric unit contains two monomers (labeled A and B), each forming a 2-layer sandwich comprising an α-helix and a three-stranded antiparallel β-sheet, distinct from the TP domain (Fig. 5C). Clear and continuous electron density allowed the modeling and unambiguous assignment of both PASTA domains (Fig. 5C). When *Sa*PASTA$_{PBP1}$ is compared with other structures deposited in the PDB using DALI (42), the top hit identified was *S. pneumoniae* PBP2x (Z-score, 15.7), showing a significant conservation of the PASTA fold despite low sequence identity (Fig. 5C). Unlike the linear arrangement observed for PASTA domains in serine/threonine kinases (43, 44), *Sa*PASTA$_{PBP1}$ adopts a compact upside-down globular arrangement (Fig. 5C). The arrangement of the two PASTA domains solved here, in isolation from the TP domain in comparison to structural analyses of *Sp*PBP2x, is entirely consistent with a nonlinear PASTA domain arrangement. First, the structures of *Sa*PASTA$_{PBP1}$ and the PASTA domains

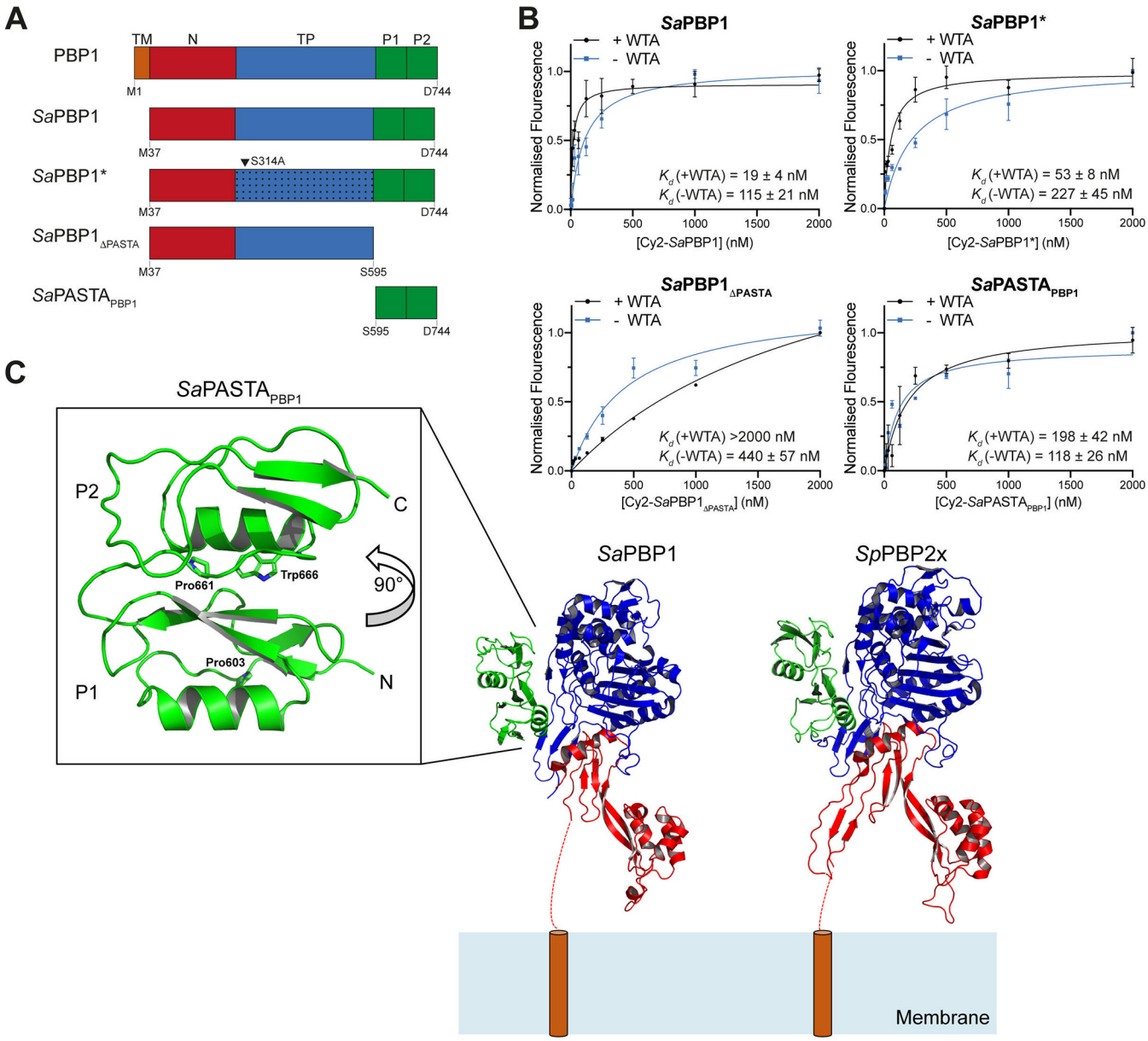

FIG 5 PBP1 PASTA domains bind cell walls. (A) Schematic representation of structural domain organization of *S. aureus* PBP1 (top) and recombinant proteins (*Sa*PBP1, *Sa*PBP1$_{\Delta PASTA}$, *Sa*PBP1*, and *Sa*PASTA$_{PBP1}$) used in this study. TM, short cytoplasmic fragment and transmembrane helix (orange); N, N-terminal pedestal domain (red); TP, transpeptidase domain (blue); P, PASTA domains (green). The arrowhead indicates the inactivation substitution in the TP domain of *Sa*PBP1*. The first and last amino acids of constructs are indicated. (B) Fluorescence cell wall sedimentation assay. A Wilcoxon signed rank test ($P < 0.05$) was carried out to assess the significance of difference in +WTA/–WTA PG binding: *Sa*PBP1, $P = 0.0273$; *Sa*PBP1*, $P = 0.0078$; *Sa*PBP1$_{\Delta PASTA}$, $P = 0.0195$; *Sa*PASTA$_{PBP1}$, $P \geq 0.9999$, not significant. Data represent the mean ± SD. Error bars that are smaller than the symbols are not shown. (C) Structure of *Sa*PASTA$_{PBP1}$. The crystal structure of *S. aureus* PBP1 lacking the PASTA domains (*Sa*PBP1, PDB 5TRO) and our *Sa*PASTA$_{PBP1}$ structure were superimposed on *S. pneumoniae* PBP2x (*Sp*PBP2x, PDB 5OAU) and displayed as cartoons. Their N termini are orientated close to the representative cell membrane, as if anchored there by their respective transmembrane helices (dashed red line/orange cylinder). Individual domains are colored as follows: N-terminal pedestal domain (red), transpeptidase domain (blue), and PASTA domain (green). The individual PASTA domains are labeled P1 and P2, respectively. Residues Pro603, Pro661, and Trp666 are displayed as sticks, with nitrogen atoms colored blue.

of *Sp*PBP2x share a pairwise root mean square deviation (RMSD) of 2.2 Å over 114 Cα, and when *Sa*PASTA$_{PBP1}$ is superimposed on the PASTA domains of *Sp*PBP2x, there are no steric clashes with the TP domain. Second, the linker between PASTAs in *Sa*PASTA$_{PBP1}$ has a sequence of DGDLTMPDMSGW, is neither glycine- nor alanine-rich, is not predicted to be disordered using the IUPred2 or ANCHOR2 web servers, and has a mean B factor of 44 Å^2 in comparison to a mean B factor of 42 Å^2 for the entire chain. Third, the interface between the PASTA domains is more reminiscent of the hydrophobic core of a globular

protein than the more polar interface observed between molecules in crystal packing. Finally, the two proline residues that apparently define PBP1 as a nonbinder of PG are found buried from solvent either at the interface of PASTA domain 1 with the TP domain (Pro603) or at the interface between the TP domain and PASTA domains 1 and 2 (Pro661). The latter interface includes the only tryptophan (Trp666) in the sequence of *Sa*PASTA$_{PBP1}$; tryptophan residues are frequent markers of carbohydrate binding sites in proteins (45), and in the absence of any obvious grooves or surface features associated with conserved sequence distributions and/or electrostatics, it remains unclear how the PASTA domains of *Sa*PBP1 recognize PG.

DISCUSSION

S. aureus has just two essential PBPs (46) and so forms an apparently simple system to understand cell wall growth and division. Even the transpeptidase activity of these two enzymes can be substituted by a single enzyme in the presence of β-lactam antibiotics via the acquisition of PBP2A, encoded by *mecA*, in MRSA strains. Our recent study has revealed that the presence of *mecA* and associated genetic lesions has a profound effect on *S. aureus*, even in the absence of antibiotics (25), leading to the discovery here that the PG biosynthetic activity of PBP1 is essential in MSSA but not in MRSA (Fig. 1D). This observation has important ramifications for many studies in *S. aureus*, where the use of an MRSA background can complicate phenotype interpretation. To understand the fundamental role of PBP1 activity in basic cell physiology, we have thus used an MSSA strain with a defined genetic background.

The essential function of PBP1 is associated with its crucial role in septal PG synthesis (14, 47). Here, we show that PBP1, in MSSA, has roles in both early and later stages of septum synthesis and can interact with other cell division components and make and bind to PG. PG binding is primarily mediated by the PASTA domains that are essential for cell division. There is clear overall structural similarity between *S. aureus* PBP1 and *S. pneumoniae* PBP2x PASTA domains in the way that the two tandem PASTA domains associate into an antiparallel bundle (Fig. 5C); this is in marked contrast to the head-to-tail linear PASTA domain repeats more typically found in STPKs. The highly hydrophobic interface between the two PASTA domains means it is unlikely to open up like butterfly wings to bind to PG; similarly, an extensive, linear interaction with PG, which is likely to occur with the head-to-tail PASTA domain arrangements seen in STPKs and which may require their dimerization (44), does not occur in *Sa*PBP1. Despite the successful production of diffracting crystals of *Sa*PASTA$_{PBP1}$ grown in the presence of PG fragments (including an *N*-acetylglucosamine:*N*-acetylmuramic acid disaccharide), none of the structures yielded electron density features consistent with the stable binding of PG fragments. There are several potential explanations, including a lack of affinity of PASTA domains for small PG fragments, unrepresentative of the sacculus of *S. aureus*; our sedimentation assay does not permit the analysis of the binding of PASTA domains to small, soluble PG precursors. Consequently, and in common with all other PASTA domain structural analyses, the molecular details of PG recognition by *Sa*PBP1 remain elusive. During the preparation of the manuscript, Martínez-Caballero et al. (27) published a crystal structure of the two PASTA domains of PBP1, also in the absence of endogenous ligand, which is indistinguishable (RMSD, 0.7 Å over 204 superimposed residues) from the structure that we report here. The same authors also solved structures of *Sa*PBP1 in the presence and absence of β-lactams and pentaglycine (in which the PASTA domains were disordered). The latter structural analysis revealed that the pentaglycine substrate mimetic is not long enough to span between the transpeptidase active site and the PASTA domains, suggesting that the PG feature(s) recognized by the PASTA domain is/are chemically more complex than a simple short polypeptide.

S. aureus is a spheroid coccus that can divide successively in orthogonal planes (30, 48). Septation is first observed as the formation of a band of PG known as the piecrust (30). This then transitions to the production of the septal plate itself, an initially V-

shaped structure with a narrower leading edge (9). After closure of the septal annulus, the now bowed septum fills out to yield the mature structure prior to septal scission. The septal plate has two distinct PG architectures with a ring-like pattern at its core, which is exposed upon scission, and a subsequently synthesized fine mesh, akin to the rest of the peripheral cell wall (5). Loss of the entire PBP1, or just its PASTA domains, does not prevent piecrust formation but does result in multi- and/or off-center piecrusts without the ability to produce the septal plate (Fig. 2F). Thus, piecrust formation does not require PBP1 but is likely the result of the activity of the essential PBP2. PBP1 may regulate division site selection through PG cell wall recognition via its PASTA domains. Alternatively, as the division apparatus is unable to progress effectively to septal plate formation due to the lack of PBP1, this may lead to further rounds of initiation and piecrust formation. PBP1 has a clear role in septal plate formation where in the absence of PBP1 or the PASTA domains, cells form aberrantly shaped septa that do not close their annuli (Fig. 2A to E). In stark contrast, inactivation of PBP1 TP activity (*pbp1**) does not stop inward septum progression, as observed with loss of PBP1 or the PASTA domains. However, such septa are misshapen, curved, and abnormally thick (Fig. 2A to E and Fig. 3). The use of the PBP1-specific antibiotic MEM at 1× MIC led to the similar morphology of thickened and misshapen septa. Two independent avenues of research both led to the conclusion that PBP1 TP activity is essential for continued division and colony formation, and while septum formation is disturbed, it is not entirely prevented. Therefore, PBP1 retains its regulatory function(s) regardless of activity loss. Loss of PBP1 activity may result in futile glycan strand synthesis (49) by its partner transglycosylase FtsW (14) and/or the continued activity of PBP2, resulting in the observed aberrant septa and stasis. FtsW in *S. aureus* is essential and required for septum progression (14). In *Bacillus subtilis* the cell division-associated PBP2B is essential, but its enzyme activity is not and can be compensated for by PBP3 (50). Here, in the *pbp3 pbp4* background loss of PBP1 activity did not lead to death of the cells (Fig. S4E and F), suggesting that the nonessential enzymes do not support survival in the absence of PBP1 TP activity, whereas deletion of the PASTA domains leads to rapid death of the cells (Fig. 1D) due to loss of protein functionality not observed in the *pbp1**. Differences in plating efficiency and rate of loss of cellular viability between Δ*pbp1* and $pbp1_{\Delta PASTA}$ may reflect aberrant function of the truncated protein. As well as binding to the cell wall, PBP1 also apparently interacts with multiple protein partners, including EzrA, DivIB/C, PBP2, and FtsW (Fig. S8A and B) (14, 35). Recently, the PASTA domains from *B. subtilis* PBP2B were shown to regulate PBP2B interaction with DivIB (51). *S. aureus* DivIB is a PG-binding protein essential for division, the depletion of which leads to septal plate formation loss (34, 35). Here, the PBP1 PASTA domains were found to be involved in binding to DivIB and FtsW, alluding to their essential role in cell division. This could be a direct interaction, or loss of PBP1 PASTA may cause a conformational change in the remaining protein, as other's data suggest the FtsW-PBP1 interaction occurs via the PBP1 stalk domain (52). FtsW is a SEDS protein whose TG activity requires the presence of PBP1. Bifunctional aPBP (including PBP2) and bPBP-SEDS (including PBP1-FtsW) pairs share similar activities, but the fact that they coexist in many bacterial species implies there is a division of responsibilities between them. Indeed, it has been proposed lately that bPBP-SEDS pairs likely lay the primary PG matrix, while aPBPs support the initial PG by modifying, filling in, and adding PG to it (53, 54). The *S. aureus* septal plate PG has two distinct architectures, a disordered mesh present on its cytoplasm facing side and a ring structure at its core, which is revealed after the cells have split (5, 30) (Fig. 6). Recent AFM analysis from *Staphylococcus warneri* also describes the distinct PG architectures during septation as piecrust and septal plate rings/mesh (55). When sacculi are purified from *S. warneri*, the septum can split apart, revealing the rings, even in septa that have not closed their annulus, showing that the rings are not a likely result of PG hydrolysis during cell scission. We hypothesize (Fig. 6) that once the piecrust has been produced, PBP1 and FtsW use this as a foundation to initiate septal plate formation. Together they make the rings of material

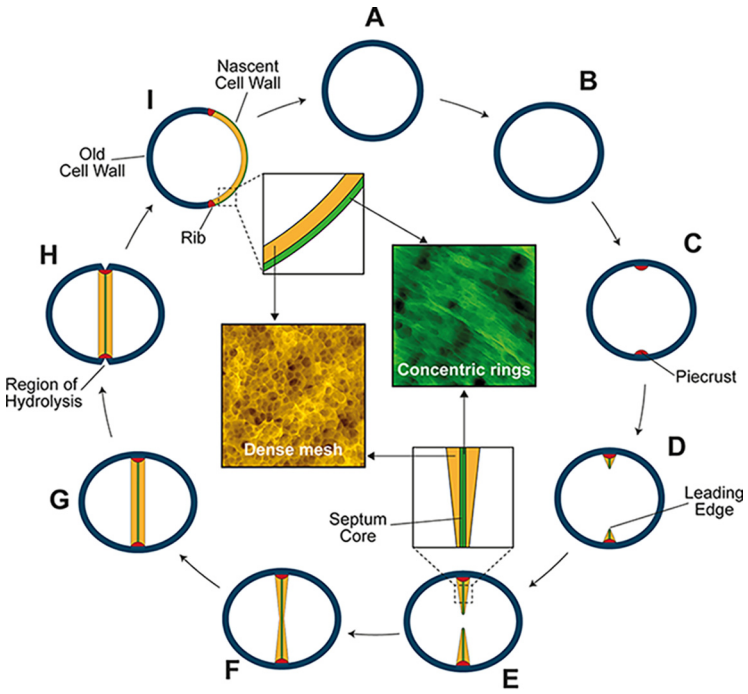

FIG 6 Conceptual model of septum formation in *S. aureus*, where PBP1 is required for septum formation and its characteristic ring-like PG architecture. (A and B) The growing *S. aureus* cell increases in volume (63). (C) Septal synthesis starts by formation of the piecrust (red) (30). This occurs as the result of the activity of PBP2 and forms the foundation for the septal plate. (D and E) The V-shaped septal plate (9) progresses inward by insertion of an initial, concentric ring-like structured PG synthesized by PBP1-FtsW at its core. Without PBP1 or PBP1 PASTA, the septal plate cannot be initiated, but in PBP1* it progresses but is aberrant. The PBP1-derived ring structure acts as a framework for the ensuing mesh-structured PG produced by PBP2. (F) The annulus closes, resulting in a bowed septum. (G) The septum is filled out by peptidoglycan insertion executed by PBP2, and this continues until the cross-wall is of uniform thickness (9). (H) The cell wall is hydrolyzed at the plane of septation. (I) Daughter cells separate. The cell wall of the daughter cell (colored insets) is a chimera of the old cell wall with both internally and externally mesh-structured PG and a nascent cell wall with the external ring-structured PG and the mesh-like cytoplasmic facing PG (5).

that become the core of the developing septum, providing the framework for PBP2 to make the bulk of the septal plate as a tight mesh alongside PBP4 and the insertion of WTA via the *tar* pathway. Loss of PBP1 TP activity in the presence of active PBP2 leads to the lack of the ring framework and aberrant, unproductive septum formation. The rings that form the center of the developing septum also provide the cleavage plane during scission.

Cell division is a fundamental requirement for life. A central question in bacteria is how is the division septum synthesized and then split to yield two daughter cells while maintaining cellular integrity in the face of internal turgor? Here, we have begun to answer this question by revealing the complex synthesis coordination mechanisms that allow this biological engineering feat to be accomplished.

MATERIALS AND METHODS

Bacterial growth conditions. The strains used in this study are listed in Table S1A.

All *Staphylococcus aureus* strains were grown in tryptic soy broth (TSB) containing appropriate antibiotics at 37°C, unless otherwise indicated, with aeration. All *Escherichia coli* strains, unless otherwise stated, were grown in Lysogeny broth (LB) containing appropriate antibiotics at temperatures ranging from 20°C to 37°C with aeration. For solid medium, 1.5% (wt/vol) agar was added. When necessary, growth medium was supplemented with kanamycin (50 μg mL^{-1}), tetracycline (1 μg mL^{-1}), chloramphenicol (10 μg mL^{-1}, *S. aureus*; 30 μg mL^{-1}, *E. coli*), erythromycin (5 μg mL^{-1}), spectinomycin (250 μg mL mL^{-1}), ampicillin (100 μg mL^{-1}), meropenem (0.4 μg mL^{-1}, 1× MIC for SH1000 WT; 0.2 μg mL^{-1}, 1× MIC for *pbp3 pbp4*), 5-bromo-4-chloro-3-indolyl β-D-thiogalactopyranoside (X-Gal; 80 μg mL^{-1}, *S. aureus*; 40 μg mL^{-1}, *E. coli*), or isopropyl β-D-thiogalactopyranoside (IPTG; 50 μM or 1 mM).

Plasmid construction. The plasmids and oligonucleotides used in this study are listed in Table S1 parts B and C, respectively.

Plasmids were cloned using *E. coli* NEB5α following previously described methods (56, 57).

pKB-*Pspac-pbp1*. A fragment containing the ribosome-binding site (RBS) and coding region of *S. aureus pbp1* was PCR amplified from the genomic DNA of *S. aureus* SH1000 using pCQ-pbp1-F/-R primers and cloned into pCQ11-FtsZ-SNAP (9) cut with NheI and AscI by Gibson assembly, resulting in pCQ11-P*spac-pbp1*. Next, the region containing P*spac*, RBS, and *pbp1* was PCR amplified from pCQ11-P*spac-pbp1* using pKB-Pspac-pbp1-F/-R primers and cloned into cloned into BamHI and EcoRI cut pKASBAR (34) by Gibson assembly, giving pKB-P*spac-pbp1*.

pMAD-Δ*pbp1*. Fragments encompassing 1-kb regions flanking upstream (from −980 bp upstream of *pbp1* to the first 20 bp of *pbp1*) and downstream (from 2,214 bp of *pbp1* to 970 bp downstream of *pbp1*) of *pbp1* were PCR amplified from *S. aureus* SH1000 genomic DNA using primer pairs pbp1-A/-B and pbp1-C/-D, respectively, and cloned into BamHI and EcoRI cut pMAD by Gibson assembly, creating deletion vector pMAD-Δ*pbp1*.

pMAD-*pbp1*$_{\Delta PASTA}$. Fragments encompassing 1.5-kb regions flanking the region encoding *pbp1* PASTA domains (upstream, from 286 bp to 1,785 bp of *pbp1*; downstream, from 2,214 bp of *pbp1* to 970 bp downstream of *pbp1*) were PCR amplified from *S. aureus* SH1000 genomic DNA using pbp1-E/-F and pbp1-G/-H primers and cloned into BamHI and EcoRI cut pMAD by Gibson assembly, resulting in deletion vector pMAD-*pbp1*$_{\Delta PASTA}$.

pMAD-*pbp1.** An ~1.3-kb fragment covering an upstream region of the active site of *pbp1* (from −334 bp upstream of *pbp1* to the first 950 bp of the *pbp1* coding sequence) and an ~1.3-kb fragment comprising the 3′ fragment of *pbp1* (930- to 2,235-bp region of *pbp1*) were PCR amplified from *S. aureus* SH1000 genomic DNA using primer pairs pbp1*5′-F/-R and pbp1*3′-F/-R, respectively. Primers pbp1*5′-R and pbp1*3′-F were designed to introduce a T to G point mutation resulting in a Ser314Ala substitution. The PCR products were ligated with pMAD cut with EcoRI and BamHI by Gibson assembly, resulting in pMAD-*pbp1**.

T25-PBP1$_{\Delta PASTA}$. A fragment carrying *S. aureus pbp1* without the PASTA domains (M1-S595) was PCR amplified from *S. aureus* SH1000 genomic DNA using T25-pbp1-F and T25-pbp1pasta-R and cloned into BamHI and EcoRI cut pKT25, resulting in T25-PBP1$_{\Delta PASTA}$.

pVR plasmids. Full-length *pbp1* (M1-D744) was *E. coli* codon optimized, synthesized with GenScript, PCR amplified using VR47F/R, and cloned into KpnI and HindIII cut pOPINRSF using In-Fusion cloning (TaKaRa Bio), resulting in pVR01. Construction of pVR02 (*Sa*PBP1, M37-D744) and pVR06 (*Sa*PASTA$_{PBP1}$, S595-D744) was performed using inverse PCR (iPCR) (58), with pVR01 as a template and primer pairs VR49F/VR49R and VR57F/VR49R, respectively. pVR03 (*Sa*PBP1*, M37-D744, S314A) and pVR04 (*Sa*PBP1$_{\Delta PASTA}$, M37-S595) were constructed with QuikChange site-directed mutagenesis of pVR02 using VR51 and VR53, respectively.

pSA50. In order to construct an overexpression plasmid for sPBP1-BAP, the A51-D744 fragment of *E. coli* codon optimized *pbp1* was PCR amplified using primers OPPF20018F/OPPF20018R and cloned into KpnI and SfoI cut pOPINJB by In-Fusion cloning (TaKaRa Bio). The resulting construct, pSA50 contains an N-terminal hexahistidine tag fused to glutathione-S-transferase followed by a human rhinovirus 3C protease site, while the PBP1 (A51-D744) C-terminal end is fused to a biotin acceptor peptide (BAP) sequence.

Construction of *S. aureus* mutants. All vectors were passed through a restriction-deficient *S. aureus* RN4220 before being transduced into a final *S. aureus* SH1000 strain. Transformation and phage transduction of *S. aureus* were carried out as described previously (59, 60).

Δ*pbp1*, *pbp1*$_{\Delta PASTA}$, and *pbp1.** For construction of *pbp1* mutation strains, first, an ectopic copy of *pbp1* under the control of the P*spac* promoter was introduced at the lipase (*geh*) locus. Electrocompetent CYL316 was transformed with pKB-P*spac-pbp1*. The chromosomal fragment containing the integrated plasmid was moved into *S. aureus* SH1000 by phage transduction, resulting in SJF4588 (*S. aureus* SH1000 *geh*::P*spac-pbp1*). Next, electrocompetent RN4220 was transformed with pMAD-Δ*pbp1*, pMAD-*pbp1*$_{\Delta PASTA}$, or pMAD-*pbp1**, and the plasmids were moved to SJF4588 by phage transduction. Integration at 42°C and excision at 28°C of pMAD-Δ*pbp1*, pMAD-*pbp1*$_{\Delta PASTA}$, or pMAD-*pbp1** resulted in strains SJF5116, SJF5275, and SJF4590, respectively. To allow controlled expression of *pbp1* from P*spac*, pGL485, a multicopy plasmid carrying *lacI* was introduced, creating strains Δ*pbp1* (*S. aureus* SH1000 *geh*::P*spac-pbp1* Δ*pbp1 lacI*), *pbp1*$_{\Delta PASTA}$ (*S. aureus* SH1000 *geh*::P*spac-pbp1 pbp1*$_{\Delta PASTA}$ *lacI*), and *pbp1** (*S. aureus* SH1000 *geh*::P*spac-pbp1 pbp1** *lacI*). On all occasions, consistent colony size and growth kinetics were monitored to prevent the selection of suppressor mutations.

MRSA Δ*pbp1* and MRSA *pbp1.** In order to construct high-level β-lactam-resistant mutants, Δ*pbp1* and *pbp1** were transformed with a phage lysate from SJF5046 (*S. aureus* SH1000 *lysA*::p*mecA rpoB*^{H929Q}) with selection for erythromycin resistance, resulting in low-level β-lactam-resistant Δ*pbp1* p*mecA* and *pbp1** p*mecA*. The low-level-resistant mutants were transduced again with the phage lysate from SJF5046 and selected for kanamycin resistance, resulting in MRSA Δ*pbp1* (*S. aureus* SH1000 *geh*::P*spac-pbp1* Δ*pbp1 lacI lysA*::p*mecA rpoB*^{H929Q}) and MRSA *pbp1* pbp1* (*S. aureus* SH1000 *geh*::P*spac-pbp1 pbp1** *lacI lysA*::p*mecA rpoB*^{H929Q}). MIC values were determined using antibiotic susceptibility tests using Etest MIC evaluator (Oxoid) strips.

***pbp3 pbp4*.** SH1000 was transduced with a phage lysate from NE420 (*S. aureus* JE2 *pbp3*::*Tn*), resulting in SH4421 (*S. aureus* SH1000 *pbp3*::*Tn*). To swap the erythromycin resistance cassette to a kanamycin cassette, SH4425 (*S. aureus* SH1000 *pbp4*::*Tn*) was transduced with a phage lysate from NE3004 (*S. aureus* RN4220 pKAN). Integration at 42°C and excision at 28°C of pKAN resulted in strain SH5115 (*S. aureus*

SH1000 *pbp4*::*kan*). SH4421 was subsequently transduced with a phage lysate from SH5115 (*S. aureus* SH1000 *pbp4*::*Tn*), resulting in *pbp3 pbp4* (SH5483; *S. aureus* SH1000 *pbp3*::*Tn pbp4*::*kan*).

Δ*pbp1 pbp4*, *pbp1*$_{\Delta PASTA}$ *pbp4*, and *pbp1* pbp4*. Δ*pbp1*, *pbp1*$_{\Delta PASTA}$, and *pbp1** were transduced with a phage lysate from SH5115 (*S. aureus* SH1000 *pbp4*::*kan*), resulting in Δ*pbp1 pbp4* (*S. aureus* SH1000 *geh*::P*spac-pbp1* Δ*pbp1 lacI pbp4*::*kan*), *pbp1*$_{\Delta PASTA}$ *pbp4* (*S. aureus* SH1000 *geh*::P*spac-pbp1 pbp1*$_{\Delta PASTA}$ *lacI pbp4*::*kan*), and *pbp1* pbp4* (*S. aureus* SH1000 *geh*::P*spac-pbp1 pbp1* lacI pbp4*::*kan*), respectively.

***pbp1* pbp3 pbp4*.** *pbp1* pbp4* (*S. aureus* SH1000 *geh*::P*spac-pbp1 pbp1* lacI pbp4*::*kan*) was transduced with a phage lysate from SH4421 (*S. aureus* SH1000 *pbp3*::*Tn*), resulting in *pbp1* pbp3 pbp4* (*S. aureus* SH1000 *geh*::P*spac-pbp1 pbp1* lacI pbp3*::*Tn pbp4*::*kan*).

Δ*pbp1 ezrA-gfp*, *pbp1*$_{\Delta PASTA}$ *ezrA-gfp*, and *pbp1* ezrA-gfp*. Δ*pbp1*, *pbp1*$_{\Delta PASTA}$, and *pbp1** were transduced with a phage lysate from JGL227 (*S. aureus* SH1000 *ezrA-gfp*+) (35), resulting in Δ*pbp1 ezrA-gfp* (*S. aureus* SH1000 *geh*::P*spac-pbp1* Δ*pbp1 lacI ezrA-gfp*), *pbp1*$_{\Delta PASTA}$ *ezrA-gfp* (*S. aureus* SH1000 *geh*::P*spac-pbp1 pbp1*$_{\Delta PASTA}$ *lacI ezrA-gfp*), and *pbp1* ezrA-gfp* (*S. aureus* SH1000 *geh*::P*spac-pbp1 pbp1* lacI ezrA-gfp*), respectively.

Δ*pbp1 tarO*, *pbp1*$_{\Delta PASTA}$ *tarO*, and *pbp1* tarO*. Δ*pbp1*, *pbp1*$_{\Delta PASTA}$, and *pbp1** were transduced with a phage lysate from *tarO* (*S. aureus* SA113 Δ*tarO*::*ery* pUC1-*tarO*) (31), resulting in Δ*pbp1 tarO* (*S. aureus* SH1000 *geh*::P*spac-pbp1* Δ*pbp1 lacI* Δ*tarO*::*ery*), *pbp1*$_{\Delta PASTA}$ *tarO* (*S. aureus* SH1000 *geh*::P*spac-pbp1 pbp1*$_{\Delta PASTA}$ *lacI* Δ*tarO*::*ery*), and *pbp1* tarO* (*S. aureus* SH1000 *geh*::P*spac-pbp1 pbp1* lacI* Δ*tarO*::*ery*), respectively.

PBP1 depletion. P*spac-pbp1* strains were grown from an optical density at 600 nm (OD_{600}) of 0.1 to the exponential phase (OD_{600} ~0.5) in TSB containing 10 μg mL^{-1} chloramphenicol and 50 μM IPTG. Cells were washed three times by centrifugation and resuspension in TSB. Washed cells were then used to inoculate TSB containing 10 μg mL^{-1} chloramphenicol. Cultures were inoculated to an OD_{600} of 0.05 for phenotypic studies and an OD_{600} of 0.005 for growth studies. For phenotypic analysis, cultures were incubated for 2 h to allow depletion of PBP1 before microscopy imaging. Control samples were grown in TSB supplemented with 10 μg mL^{-1} chloramphenicol and 1 mM (50 μM, *ezrA-gfp* mutants) IPTG.

For the plating efficiency test, cells grown in the presence of 10 μg mL^{-1} chloramphenicol and 50 μM IPTG to the exponential phase (OD_{600}, ~0.5) were washed three times in phosphate-buffered saline (PBS). Serial dilutions of washed cells were plated on TSB containing 10 μg mL^{-1} chloramphenicol, with or without 1 mM IPTG. Relative plating efficiency (% CFU) is expressed as the number of cells that grow on plates without IPTG ($CFU_{no\ IPTG}$) to cells that grow in the presence of IPTG (CFU_{IPTG}) multiplied by 100%:

$$\%CFU = \frac{CFU_{no\ \ IPTG}}{CFU_{IPTG}} \times 100\%$$

Meropenem activity assays. *S. aureus* strains were grown overnight in TSB. The overnight cultures were used to inoculate fresh TSB medium to an OD_{600} of 0.05. When cells reached an OD_{600} of 0.2 to 0.4, meropenem was added, and the change of bacterial count was monitored. The CFU per mL of culture measures were normalized to the initial CFU/mL at the time of the antibiotic addition, at time zero (t_0).

$$Relative\ \ CFU/mL = \frac{CFU/mL_{tn}}{CFU/mL_{t0}}$$

For phenotypic analysis, cells were treated for 1 h with 1× MIC meropenem before microscopy imaging.

Fractionation of *S. aureus* membranes. The membrane fraction of *S. aureus* was prepared as previously described (61) with the following modifications. *S. aureus* cells grown to the appropriate growth phase were recovered by centrifugation (5,000 × *g*, 10 min, 4°C) and washed three times by resuspension and centrifugation (5,000 × *g*, 10 min, 4°C) in PBS. Cells were resuspended in 50 mM Tris, 100 mM NaCl, pH 8.0 containing Complete Protease Inhibitor (Roche) and broken using 0.1-mm silica spheres (lysing matrix B) and FastPrep homogenizer (MP Biomedicals) in 12 cycles of 30 s, at maximum speed (6.5 m s^{-1}), with 5 min of incubation on ice between cycles. Cell lysates were centrifuged (8,000 × *g*, 10 min, 4°C) to remove unbroken cells. The supernatant was then spun (8,000 × *g*, 10 min, 4°C) to sediment cell wall material. The membrane fraction was recovered from the supernatant by centrifugation (35,000 × *g*, 20 min, 4°C), and the pellet (membranes) was resuspended in PBS. The total protein concentration was estimated by Bradford assay.

***In vitro* labeling of *S. aureus* PBPs with BocillinFL.** This method was adopted from a published protocol (62) with minor modifications. Membrane proteome samples (25 μg in 20 μL PBS) and purified proteins (2.5 μg in 25 μL HEPES pH 7.5 150 mM NaCl) were incubated with 25 μM BocillinFL (Invitrogen) for 20 min at 37°C. Additionally, for the competition assay, purified *Sa*PBP1 was mixed with 2.5 μg (~286 μM final concentration) ampicillin and incubated at 37°C for 10 min prior to the addition of BocillinFL. The reaction was stopped by the addition of 5× SDS-PAGE loading buffer. Membrane proteome was additionally incubated for 10 min at 90°C. The samples were run on a 6 to 20% (wt/vol) SDS-PAGE gradient or 10% (wt/vol) SDS-PAGE gel and visualized using a Bio-Rad ChemiDoc MP imaging system or a GE Typhoon FLA 9500.

Labeling *S. aureus* D-amino acids. *S. aureus* cells were incubated with 500 μM (2 mM for *pbp4* mutants) HADA or 1 mM ADA-DA at 37°C for 5 min. Cells were then washed by centrifugation and resuspension in PBS.

Click chemistry. ADA-DA containing an azide functional group was fluorescently labeled with Atto 488 alkyne at 5 μg mL^{-1} via the click reaction [copper (I)-catalyzed alkyne-azide cycloaddition]. This was carried out using the Click-iT cell reaction buffer kit (Thermo Fisher) according to the manufacturer's protocol.

Labeling *S. aureus* with fluorescent NHS-ester. Fixed cell wells were resuspended in PBS containing 8 μg mL^{-1} Alexa Fluor 555 NHS-ester (Invitrogen) and incubated at room temperature for 30 min. Cells were washed twice by centrifugation and resuspension in PBS.

Fixing for fluorescence microscopy. Cells were fixed by incubation in 1.6% (wt/vol) paraformaldehyde at room temperature for 30 min.

Fluorescence microscopy. Fixed cells were dried onto a poly L-lysine-coated slide, mounted in PBS, and imaged on a Nikon Ti inverted microscope fitted with a Lumencor Spectra X light engine. Images were taken using a 100× PlanApo (1.4 NA) oil objective using 1.518 RI oil and detected by an Andor Zyla sCMOS camera.

Cell volume estimation. Cell volume calculations were carried out as previously described (63). The long and short axes of cells were measured using Fiji. The volume was then calculated based on a prolate spheroid shape with volume

$$V = 4/3\pi ab^2,$$

where *a* and *b* are the radii along the long and short axes, respectively.

Transmission electron microscopy. *S. aureus* strains were prepared for electron microscopy as previously described (64).

Preparation of *S. aureus* sacculi. Peptidoglycan from *S. aureus* cells was extracted and, if required, hydrofluoric acid (HF)-treated to remove cell wall accessory polymers as previously described (64).

Sacculi immobilization for AFM imaging. The immobilization surface was prepared by adding the solution mixed with 171 μL of 100 mM $NaHCO_3$, 3 μL of 1 M NaOH, and 6 μL of Cell-Tak (Corning, 5% [wt/vol] in acetic acid) on freshly cleaved mica. After 30 min of incubation, the surface was washed with 5 × 200 μL high-pressure liquid chromatography (HPLC)-grade water. Sacculi stocks were 10 times diluted in HPLC-grade water and briefly tip-sonicated to resuspend them prior to immobilization. Then, 10 μL of the sacculi suspension was added to 40 μL of HPLC-grade water on the Cell-Tak immobilization surface and incubated for 1 h. The surface was then thoroughly rinsed with HPLC-grade water, blow-dried with nitrogen, and stored in a petri dish at room temperature before AFM imaging.

AFM Imaging and image analysis. AFM imaging was carried out on a Nanowizard III ULTRA Speed system (JPK, Germany). Rectangular cantilevers with a nominal spring constant of 0.3 N/m and resonant frequency (in liquid) of ~150 kHz (USC-F0.3-k0.3; NanoWorld, Switzerland) were used. The spring constant and deflection sensitivity of each cantilever were calibrated prior to each measurement (65, 66) Measurements were carried out in quantitative imaging mode at room temperature in the buffer composed of 200 mM KCl and 10 mM Tris. Scans were driven at a line rate of ~0.78 Hz, with a typical Z length of 300 nm and trigger force of 20 nN. The resultant topographic images were processed using JPK Data Processing. No flattening or surface subtraction was applied. A high-pass filter (scale: 100% to 500%, degree of smoothing: 5 px, horizontal) was applied to the higher magnification images to enhance the contrast without modifying the morphological features. The morphological features of sacculi were summarized from images obtained on abundant technical repeats of 2 biological replicates.

Recombinant protein production and purification. sPBP1-BAP. *E. coli* BL21(DE3) cells containing plasmid pSA50 were grown in LB medium supplemented with 100 μg mL^{-1} ampicillin at 37°C to an OD_{578} of 0.5. Protein overproduction was induced by addition of 0.5 mM IPTG to the cell culture and further incubation for 4 h at 30°C. Cells were harvested by centrifugation (6,200 × *g*, 15 min, 4°C), and the pellet was resuspended in basic buffer (25 mM Tris-HCl, 100 mM NaCl, pH 7.5). After addition of 1 mM phenylmethylsulfonyl fluoride (PMSF), a 1:1,000 dilution of protease inhibitor cocktail (Sigma-Aldrich), and DNase, the cells were disrupted by sonication (Branson digital sonifier). The cell lysate was centrifuged (130,000 × *g*, 60 min, 4°C), and the supernatant was recovered. The supernatant was incubated with Ni-NTA Superflow (Qiagen) for 2 h at 4°C with gentle stirring, which had been preequilibrated in basic buffer. The resin was poured into a gravity column and washed with 20 volumes of wash buffer (25 mM Tris-HCl, 150 mM NaCl, 10% [vol/vol] glycerol, 10 mM $MgCl_2$, 20 mM imidazole, pH 7.5). Bound protein was eluted with elution buffer (25 mM Tris-HCl, 150 mM NaCl, 10% [vol/vol] glycerol, 10 mM $MgCl_2$, 600 mM imidazole, pH 7.5). Next, 10 U mL^{-1} of HRV-3C protease (TaKaRa) was added to the Ni-NTA-eluted protein to remove the oligohistidine-GST tag during dialysis against 3 L of dialysis buffer I (25 mM Tris-HCl, 150 mM NaCl, 10 mM EGTA, 10% [vol/vol] glycerol, pH 7.5) for 20 h at 4°C. Digested protein was dialyzed against 3 L of dialysis buffer II (25 mM Tris-HCl, 150 mM NaCl, 10 mM $MgCl_2$, 10% [vol/vol] glycerol, pH 7.5), for 3 h at 4°C. The protein was incubated in the same Ni-NTA beads (preequilibrated in dialysis buffer II) for 2 h at 4°C to remove the contaminants and the His-GST tag from the sample. The flowthrough and the washes (2 volumes of wash buffer) were pooled, dialyzed against storage buffer (25 mM HEPES-NaOH, 150 mM NaCl, 10 mM $MgCl_2$, 10% [vol/vol] glycerol, pH 7.5), and concentrated using a Vivaspin Turbo 15 column (molecular weight cutoff [MWCO] of 50,000 Da).

***Sa*PBP1, *Sa*PBP1*, *Sa*PBP1$_{\Delta PASTA}$, and *Sa*PASTA$_{PBP1}$.** All recombinant proteins were produced in *E. coli* Rosetta (DE3) cells at 37°C in Terrific Broth (TB) medium supplemented with 50 μg mL^{-1} kanamycin and 30 μg mL^{-1} chloramphenicol. Once cultures had reached an OD_{600} of 0.9, protein expression was induced with 1 mM IPTG for 20 h at 20°C. Cells were harvested by centrifugation (4,000 × *g* at 4°C for 30 min), and the pellet was resuspended in a buffer of 50 mM Tris-HCl, pH 8.0, 500 mM NaCl, 20 mM imidazole supplemented with one EDTA-free protease inhibitor cocktail tablet (Roche), and DNase (4 μg mL^{-1}

final concentration). The cells in this resuspension were lysed by two passes through a One-Shot cell disruptor (Constant Systems) at 23 kilopounds per square inch (kpsi), and the cell debris was removed by centrifugation (40,000 × *g* at 4°C for 30 min). The first purification step was affinity chromatography with a 5-mL HisTrap FF column (GE Healthcare) precharged with Ni^{2+} and equilibrated in buffer A (50 mM Tris-HCl, pH 8.0, 500 mM NaCl, 20 mM imidazole). A linear concentration gradient of imidazole was applied to elute the protein using buffer B (50 mM Tris-HCl, pH 8.0, 500 mM NaCl, 800 mM imidazole). Further purification was carried out by size exclusion chromatography using a Superdex 200 Hi Load 16/60 column (GE Healthcare). Proteins were eluted with SEC buffer (25 mM Tris-HCl, pH 8.0, 150 mM NaCl) and analyzed by SDS-PAGE.

Generation of anti-PBP1 antibody. Serum against sPBP1A-BAP was produced from rabbits following a 28-day immunization program at Eurogentec (Belgium), and it was purified as previously described (67).

Immunoblot analysis. *S. aureus* cultures were washed three times by resuspension and centrifugation (5,000 × *g*, 10 min, 4°C) in PBS. Cells were resuspended in TBSI (50 mM Tris, 100 mM NaCl, pH 8.0, plus Complete Protease Inhibitor Cocktail [Roche]) and broken using 0.1 mm silica spheres (lysing matrix B) and FastPrep homogenizer (MP Biomedicals) in 12 cycles of 30 s, at maximum speed (6.5 m s^{-1}), with a 5-min incubation on ice between cycles. Cell lysates were centrifuged (5,000 × *g*, 10 min, 4°C) to remove unbroken cells. Approximately 60 μg of total protein was separated on a 12% (wt/vol) SDS-PAGE gel and electroblotted onto a nitrocellulose membrane and blocked in 5% (wt/vol) skimmed milk in TBST (20 mM Tris-HCl, pH 7.6, 17 mM NaCl, 0.1% [vol/vol] Tween 20). The membrane was incubated with primary polyclonal anti-PBP1 (1:1,000) overnight with gentle agitation at 4°C. Primary antibodies were detected using horseradish peroxidase-conjugated goat anti-rabbit IgG (1:10,000; Bio-Rad) and Clarity Western enhanced chemiluminescence (ECL) substrate (Bio-Rad) reagent according to the manufacturer's protocol. Chemiluminescence was detected using a Syngene G:BOX Chemi XX9 system.

Crystallization, data collection, and structure determination. Crystallization of *Sa*PASTA$_{PBP1}$ was carried out at 20°C by the sitting-drop vapor diffusion method in 96-well MRC plates (Molecular Dimensions) with a Mosquito crystallization robot (TTP LabTech) and commercial crystallization screens (Hampton Research and Molecular Dimensions). Orthorhombic crystals of diffraction quality, with a maximum dimension of approximately 500 μm, appeared overnight from a mixture of equal volumes of protein solution (42 mg mL^{-1} in 25 mM Tris-HCl, pH 8.0, 150 mM NaCl) and reservoir solution (0.2 M NaCl, 0.1 M sodium/potassium phosphate, pH 6.2, 50% [vol/vol] polyethylene glycol [PEG] 200). Diffraction data were indexed and integrated using XDS (68) and scaled using AIMLESS (69) from the CCP4 program suite (70). The crystals displayed space group $P2_12_12_1$ with unit cell lengths a = 39.8 Å, b = 81.4 Å, and c = 89.6 Å. The asymmetric unit consisted of two polypeptide chains with an estimated solvent content of 45% and a V_m (Matthew's coefficient) of 2.24 $Å^3$/Da. The region corresponding to the two PASTA domains in the crystal structure of *S. pneumoniae* PBP2x (PBP 5OAU) was used as a molecular replacement search model, sharing approximately 26% sequence identity with *Sa*PASTA$_{PBP1}$. The search model was generated using phenix.sculptor (71) to remove nonmacromolecular chains and prune sidechains. The structure was solved by molecular replacement using PHASER (72), and the resultant electron density map was of high quality, allowing the tracing of the main chain. Model building and refinement were carried out with Coot (73) and Phenix (74), respectively. Assessments of the geometry and validation of the final model were carried out using MolProbity (75). Analyses of surface areas and interactions were made using the PISA web service (76). The graphics program PyMOL (Schrödinger, LLC) was used to generate all molecular figures presented.

Cell wall binding assays. Cell wall binding assays of recombinant PBP1 proteins fluorescently labeled with Cy2 bis-reactive dye (GE Healthcare) were performed as previously described (34), except for the binding buffer: 25 mM HEPES (pH 7.5), 150 mM NaCl, and 10 mM $MgCl_2$. Cy2-labeled cytochrome *c* (Cy2-CytC) was included as a negative control. Binding of fluorescently labeled proteins was determined by fluorescence measurements using a Hidex Sense plate reader (excitation at 490/20 nm and emission at 535/20 nm).

Bacterial two-hybrid assay. Competent BTH101 was cotransformed with pKT25 and pUT18 derivatives. Transformants were selected on LB agar plates containing 100 μg mL^{-1} ampicillin, 50 μg mL^{-1} kanamycin, and 40 μg mL^{-1} X-Gal and incubated at 30°C. Single colonies were grown in 150 μL LB with 100 μg mL^{-1} ampicillin, 50 μg mL^{-1} kanamycin, and 0.5 mM IPTG at 30°C.

To qualitatively measure for pairwise interactions, 5 μL of each overnight culture was spotted onto LB agar plates containing 100 μg mL^{-1} ampicillin, 50 μg mL^{-1} kanamycin, 0.5 mM IPTG, and 40 μg mL^{-1} X-Gal. The plates were incubated at 30°C for 24 to 48 h in an environment protected from light and imaged. To quantify interactions, overnight cultures were assayed for β-galactosidase activity against MUG (4-methylumbelliferyl-β-D-galactopyranoside) using an assay as previously described (35).

Data availability. All study data are included in the article and/or supporting information. The data that support the findings of this study are available in the Online Research Data figshare from the University of Sheffield with the identifier https://figshare.shef.ac.uk/collections/Penicillin-Binding_Protein_1_PBP1_of_Staphylococcus_aureus_Has_Multiple_Essential_Functions_in_Cell_Division/5656339/1. The crystal structure of the *S. aureus* PBP1 PASTA domains (PDB ID 7O61) can be accessed at https://www.rcsb.org/structure/7O61.

SUPPLEMENTAL MATERIAL

Supplemental material is available online only.

FIG S1, TIF file, 1.6 MB.

FIG S2, TIF file, 1.3 MB.

FIG S3, TIF file, 2.5 MB.
FIG S4, TIF file, 2 MB.
FIG S5, TIF file, 1.3 MB.
FIG S6, TIF file, 2.2 MB.
FIG S7, TIF file, 1.9 MB.
FIG S8, TIF file, 1.1 MB.
TABLE S1, DOCX file, 0.05 MB.

ACKNOWLEDGMENTS

This work was funded by the Medical Research Council (MR/N002679/1; MR/K015753/1), the UKRI Strategic Priorities Fund (EP/T002778/1), and the Wellcome Trust (212197/Z/19/Z).

L.L. thanks The Florey Institute for her Ph.D. studentship.

We gratefully acknowledge the Wolfson Light Microscopy facility for their support and assistance in this work. We thank Diamond Light Source for access to the beamline I24 (mx18598) and Arnaud Baslé for data collection, help with figure generation, and support. We are grateful to Joshua Sutton, Grace Pidwill, Victoria Lund, Laia Pasquina-Lemonche, and Chris Hill for help and advice.

We declare no competing interests.

REFERENCES

1. Vollmer W, Blanot D, de Pedro MA. 2008. Peptidoglycan structure and architecture. FEMS Microbiol Rev 32:149–167. https://doi.org/10.1111/j.1574-6976.2007.00094.x.
2. Silhavy TJ, Kahne D, Walker S. 2010. The bacterial cell envelope. Cold Spring Harb Perspect Biol 2:a000414. https://doi.org/10.1101/cshperspect.a000414.
3. Turner RD, Vollmer W, Foster SJ. 2014. Different walls for rods and balls: the diversity of peptidoglycan. Mol Microbiol 91:862–874. https://doi.org/10.1111/mmi.12513.
4. Typas A, Banzhaf M, Gross CA, Vollmer W. 2011. From the regulation of peptidoglycan synthesis to bacterial growth and morphology. Nat Rev Microbiol 10:123–136. https://doi.org/10.1038/nrmicro2677.
5. Pasquina-Lemonche L, Burns J, Turner RD, Kumar S, Tank R, Mullin N, Wilson JS, Chakrabarti B, Bullough PA, Foster SJ, Hobbs JK. 2020. The architecture of the Gram-positive bacterial cell wall. Nature 582:294–297. https://doi.org/10.1038/s41586-020-2236-6.
6. Zapun A, Contreras-Martel C, Vernet T. 2008. Penicillin-binding proteins and beta-lactam resistance. FEMS Microbiol Rev 32:361–385. https://doi.org/10.1111/j.1574-6976.2007.00095.x.
7. Schneider T, Sahl H-G. 2010. An oldie but a goodie: cell wall biosynthesis as antibiotic target pathway. Int J Med Microbiol 300:161–169. https://doi.org/10.1016/j.ijmm.2009.10.005.
8. Pinho MG, Kjos M, Veening J-W. 2013. How to get (a)round: mechanisms controlling growth and division of coccoid bacteria. Nat Rev Microbiol 11:601–614. https://doi.org/10.1038/nrmicro3088.
9. Lund VA, Wacnik K, Turner RD, Cotterell BE, Walther CG, Fenn SJ, Grein F, Wollman AJ, Leake MC, Olivier N, Cadby A, Mesnage S, Jones S, Foster SJ. 2018. Molecular coordination of Staphylococcus aureus cell division. Elife 7:e32057. https://doi.org/10.7554/eLife.32057.
10. Pinho MG, Errington J. 2005. Recruitment of penicillin-binding protein PBP2 to the division site of Staphylococcus aureus is dependent on its transpeptidation substrates. Mol Microbiol 55:799–807. https://doi.org/10.1111/j.1365-2958.2004.04420.x.
11. Pinho MG, Filipe SR, de Lencastre H, Tomasz A. 2001. Complementation of the essential peptidoglycan transpeptidase function of penicillin-binding protein 2 (PBP2) by the drug resistance protein PBP2A in Staphylococcus aureus. J Bacteriol 183:6525–6531. https://doi.org/10.1128/JB.183.22.6525-6531.2001.
12. Pereira SFF, Henriques AO, Pinho MG, de Lencastre H, Tomasz A. 2007. Role of PBP1 in cell division of Staphylococcus aureus. J Bacteriol 189:3525–3531. https://doi.org/10.1128/JB.00044-07.
13. Meeske AJ, Riley EP, Robins WP, Uehara T, Mekalanos JJ, Kahne D, Walker S, Kruse AC, Bernhardt TG, Rudner DZ. 2016. SEDS proteins are a widespread family of bacterial cell wall polymerases. Nature 537:634–638. 7622. https://doi.org/10.1038/nature19331.
14. Reichmann NT, Tavares AC, Saraiva BM, Jousselin A, Reed P, Pereira AR, Monteiro JM, Sobral RG, VanNieuwenhze MS, Fernandes F, Pinho MG. 2019. SEDS-bPBP pairs direct lateral and septal peptidoglycan synthesis in Staphylococcus aureus. Nat Microbiol 4:1368–1377. https://doi.org/10.1038/s41564-019-0437-2.
15. Taguchi A, Welsh MA, Marmont LS, Lee W, Sjodt M, Kruse AC, Kahne D, Bernhardt TG, Walker S. 2019. FtsW is a peptidoglycan polymerase that is functional only in complex with its cognate penicillin-binding protein. Nat Microbiol 4:587–594. https://doi.org/10.1038/s41564-018-0345-x.
16. Loskill P, Pereira PM, Jung P, Bischoff M, Herrmann M, Pinho MG, Jacobs K. 2014. Reduction of the peptidoglycan crosslinking causes a decrease in stiffness of the Staphylococcus aureus cell envelope. Biophys J 107:1082–1089. https://doi.org/10.1016/j.bpj.2014.07.029.
17. Srisuknimit V, Qiao Y, Schaefer K, Kahne D, Walker S. 2017. Peptidoglycan cross-linking preferences of Staphylococcus aureus penicillin-binding proteins have implications for treating MRSA infections. J Am Chem Soc 139:9791–9794. https://doi.org/10.1021/jacs.7b04881.
18. Neuhaus FC, Baddiley J. 2003. A continuum of anionic charge: structures and functions of D-alanyl-teichoic acids in gram-positive bacteria. Microbiol Mol Biol Rev 67:686–723. https://doi.org/10.1128/MMBR.67.4.686-723.2003.
19. Swoboda JG, Campbell J, Meredith TC, Walker S. 2010. Wall teichoic acid function, biosynthesis, and inhibition. Chembiochem 11:35–45. https://doi.org/10.1002/cbic.200900557.
20. Weidenmaier C, Peschel A, Xiong Y-Q, Kristian SA, Dietz K, Yeaman MR, Bayer AS. 2005. Lack of wall teichoic acids in Staphylococcus aureus leads to reduced interactions with endothelial cells and to attenuated virulence in a rabbit model of endocarditis. J Infect Dis 191:1771–1777. https://doi.org/10.1086/429692.
21. Campbell J, Singh AK, Santa Maria JP, Kim Y, Brown S, Swoboda JG, Mylonakis E, Wilkinson BJ, Walker S. 2011. Synthetic lethal compound combinations reveal a fundamental connection between wall teichoic acid and peptidoglycan biosyntheses in Staphylococcus aureus. ACS Chem Biol 6:106–116. https://doi.org/10.1021/cb100269f.
22. Farha MA, Leung A, Sewell EW, D'Elia MA, Allison SE, Ejim L, Pereira PM, Pinho MG, Wright GD, Brown ED. 2013. Inhibition of WTA synthesis blocks the cooperative action of PBPs and sensitizes MRSA to β-lactams. ACS Chem Biol 8:226–233. https://doi.org/10.1021/cb300413m.

23. Atilano ML, Pereira PM, Yates J, Reed P, Veiga H, Pinho MG, Filipe SR. 2010. Teichoic acids are temporal and spatial regulators of peptidoglycan cross-linking in Staphylococcus aureus. Proc Natl Acad Sci U S A 107:18991–18996. https://doi.org/10.1073/pnas.1004304107.
24. Pinho MG, de Lencastre H, Tomasz A. 2001. An acquired and a native penicillin-binding protein cooperate in building the cell wall of drug-resistant staphylococci. Proc Natl Acad Sci U S A 98:10886–10891. https://doi.org/10.1073/pnas.191260798.
25. Panchal VV, Griffiths C, Mosaei H, Bilyk B, Sutton JAF, Carnell OT, Hornby DP, Green J, Hobbs JK, Kelley WL, Zenkin N, Foster SJ. 2020. Evolving MRSA: high-level β-lactam resistance in Staphylococcus aureus is associated with RNA Polymerase alterations and fine tuning of gene expression. PLoS Pathog 16:e1008672. https://doi.org/10.1371/journal.ppat.1008672.
26. Yeats C, Finn RD, Bateman A. 2002. The PASTA domain: a beta-lactam-binding domain. Trends Biochem Sci 27:438. https://doi.org/10.1016/s0968-0004(02)02164-3.
27. Martínez-Caballero S, Mahasenan KV, Kim C, Molina R, Feltzer R, Lee M, Bouley R, Hesek D, Fisher JF, Muñoz IG, Chang M, Mobashery S, Hermoso JA. 2021. Integrative structural biology of the penicillin-binding protein-1 from Staphylococcus aureus, an essential component of the divisome machinery. Comput Struct Biotechnol J 19:5392–5405. https://doi.org/10.1016/j.csbj.2021.09.018.
28. Maurer P, Todorova K, Sauerbier J, Hakenbeck R. 2012. Mutations in Streptococcus pneumoniae penicillin-binding protein 2x: importance of the C-terminal penicillin-binding protein and serine/threonine kinase-associated domains for beta-lactam binding. Microb Drug Resist 18:314–321. https://doi.org/10.1089/mdr.2012.0022.
29. Kuru E, Radkov A, Meng X, Egan A, Alvarez L, Dowson A, Booher G, Breukink E, Roper DI, Cava F, Vollmer W, Brun Y, VanNieuwenhze MS. 2019. Mechanisms of incorporation for D-amino acid probes that target peptidoglycan biosynthesis. ACS Chem Biol 14:2745–2756. https://doi.org/10.1021/acschembio.9b00664.
30. Turner RD, Ratcliffe EC, Wheeler R, Golestanian R, Hobbs JK, Foster SJ. 2010. Peptidoglycan architecture can specify division planes in Staphylococcus aureus. Nat Commun 1:26. https://doi.org/10.1038/ncomms1025.
31. Salamaga B, Kong L, Pasquina-Lemonche L, Lafage L, M von und Zur M, Gibson JF, Grybchuk D, Tooke AK, Panchal V, Culp EJ, Tatham E, O'Kane ME, Catley TE, Renshaw SA, Wright GD, Plevka P, Bullough PA, Han A, Hobbs JK, Foster SJ. 2021. Demonstration of the role of cell wall homeostasis in Staphylococcus aureus growth and the action of bactericidal antibiotics. Proc Natl Acad Sci U S A 118:e2106022118. https://doi.org/10.1073/pnas.2106022118.
32. Berti AD, Sakoulas G, Nizet V, Tewhey R, Rose WE. 2013. β-Lactam antibiotics targeting PBP1 selectively enhance daptomycin activity against methicillin-resistant Staphylococcus aureus. Antimicrob Agents Chemother 57:5005–5012. https://doi.org/10.1128/AAC.00594-13.
33. Yang Y, Bhachech N, Bush K. 1995. Biochemical comparison of imipenem, meropenem and biapenem: permeability, binding to penicillin-binding proteins, and stability to hydrolysis by beta-lactamases. J Antimicrob Chemother 35:75–84. https://doi.org/10.1093/jac/35.1.75.
34. Bottomley AL, Kabli AF, Hurd AF, Turner RD, Garcia-Lara J, Foster SJ. 2014. Staphylococcus aureus DivIB is a peptidoglycan-binding protein that is required for a morphological checkpoint in cell division. Mol Microbiol https://doi.org/10.1111/mmi.12813.
35. Steele VR, Bottomley AL, Garcia-Lara J, Kasturiarachchi J, Foster SJ. 2011. Multiple essential roles for EzrA in cell division of Staphylococcus aureus. Mol Microbiol 80:542–555. https://doi.org/10.1111/j.1365-2958.2011.07591.x.
36. Schlag M, Biswas R, Krismer B, Kohler T, Zoll S, Yu W, Schwarz H, Peschel A, Götz F. 2010. Role of staphylococcal wall teichoic acid in targeting the major autolysin Atl. Mol Microbiol 75:864–873. https://doi.org/10.1111/j.1365-2958.2009.07007.x.
37. Shah IM, Laaberki M-H, Popham DL, Dworkin J. 2008. A eukaryotic-like Ser/Thr kinase signals bacteria to exit dormancy in response to peptidoglycan fragments. Cell 135:486–496. https://doi.org/10.1016/j.cell.2008.08.039.
38. Mir M, Asong J, Li X, Cardot J, Boons G-J, Husson RN. 2011. The extracytoplasmic domain of the Mycobacterium tuberculosis Ser/Thr kinase PknB binds specific muropeptides and is required for PknB localization. PLoS Pathog 7:e1002182. https://doi.org/10.1371/journal.ppat.1002182.
39. Squeglia F, Marchetti R, Ruggiero A, Lanzetta R, Marasco D, Dworkin J, Petoukhov M, Molinaro A, Berisio R, Silipo A. 2011. Chemical basis of peptidoglycan discrimination by PrkC, a key kinase involved in bacterial resuscitation from dormancy. J Am Chem Soc 133:20676–20679. https://doi.org/10.1021/ja208080r.
40. Calvanese L, Falcigno L, Squeglia F, D'Auria G, Berisio R. 2017. Structural and dynamic features of PASTA domains with different functional roles. J Biomol Struct Dyn 35:2293–2300. https://doi.org/10.1080/07391102.2016.1217274.
41. Bernardo-García N, Mahasenan KV, Batuecas MT, Lee M, Hesek D, Petráčková D, Doubravová L, Branny P, Mobashery S, Hermoso JA. 2018. Allostery, recognition of nascent peptidoglycan, and cross-linking of the cell wall by the essential penicillin-binding protein 2x of Streptococcus pneumoniae. ACS Chem Biol 13:694–702. https://doi.org/10.1021/acschembio.7b00817.
42. Holm L. 2020. DALI and the persistence of protein shape. Protein Sci 29:128–140. https://doi.org/10.1002/pro.3749.
43. Ruggiero A, Squeglia F, Marasco D, Marchetti R, Molinaro A, Berisio R. 2011. X-ray structural studies of the entire extracellular region of the serine/threonine kinase PrkC from Staphylococcus aureus. Biochem J 435:33–41. https://doi.org/10.1042/BJ20101643.
44. Barthe P, Mukamolova GV, Roumestand C, Cohen-Gonsaud M. 2010. The structure of PknB extracellular PASTA domain from Mycobacterium tuberculosis suggests a ligand-dependent kinase activation. Structure 18:606–615. https://doi.org/10.1016/j.str.2010.02.013.
45. Hudson KL, Bartlett GJ, Diehl RC, Agirre J, Gallagher T, Kiessling LL, Woolfson DN. 2015. Carbohydrate-aromatic interactions in proteins. J Am Chem Soc 137:15152–15160. https://doi.org/10.1021/jacs.5b08424.
46. Reed P, Atilano ML, Alves R, Hoiczyk E, Sher X, Reichmann NT, Pereira PM, Roemer T, Filipe SR, Pereira-Leal JB, Ligoxygakis P, Pinho MG. 2015. Staphylococcus aureus survives with a minimal peptidoglycan synthesis machine but sacrifices virulence and antibiotic resistance. PLoS Pathog 11:e1004891. https://doi.org/10.1371/journal.ppat.1004891.
47. Pereira SFF, Henriques AO, Pinho MG, de Lencastre H, Tomasz A. 2009. Evidence for a dual role of PBP1 in the cell division and cell separation of Staphylococcus aureus. Mol Microbiol 72:895–904. https://doi.org/10.1111/j.1365-2958.2009.06687.x.
48. Saraiva BM, Sorg M, Pereira AR, Ferreira MJ, Caulat LC, Reichmann NT, Pinho MG. 2020. Reassessment of the distinctive geometry of Staphylococcus aureus cell division. 1. Nat Commun 11:4097. https://doi.org/10.1038/s41467-020-17940-9.
49. Cho H, Uehara T, Bernhardt TG. 2014. Beta-lactam antibiotics induce a lethal malfunctioning of the bacterial cell wall synthesis machinery. Cell 159:1300–1311. https://doi.org/10.1016/j.cell.2014.11.017.
50. Sassine J, Xu M, Sidiq KR, Emmins R, Errington J, Daniel RA. 2017. Functional redundancy of division specific penicillin-binding proteins in Bacillus subtilis. Mol Microbiol 106:304–318. https://doi.org/10.1111/mmi.13765.
51. Morales Angeles D, Macia-Valero A, Bohorquez LC, Scheffers D-J. 2020. The PASTA domains of Bacillus subtilis PBP2B strengthen the interaction of PBP2B with DivIB. Microbiology (Reading) 166:826–836. https://doi.org/10.1099/mic.0.000957.
52. Sjodt M, Rohs PDA, Gilman MSA, Erlandson SC, Zheng S, Green AG, Brock KP, Taguchi A, Kahne D, Walker S, Marks DS, Rudner DZ, Bernhardt TG, Kruse AC. 2020. Structural coordination of polymerization and crosslinking by a SEDS–bPBP peptidoglycan synthase complex. Nat Microbiol 5:813–820. https://doi.org/10.1038/s41564-020-0687-z.
53. Cho H, Wivagg CN, Kapoor M, Barry Z, Rohs PDA, Suh H, Marto JA, Garner EC, Bernhardt TG. 2016. Bacterial cell wall biogenesis is mediated by SEDS and PBP polymerase families functioning semi-autonomously. 10. Nat Microbiol 1:1–8. https://doi.org/10.1038/nmicrobiol.2016.172.
54. Straume D, Piechowiak KW, Olsen S, Stamsås GA, Berg KH, Kjos M, Heggenhougen MV, Alcorlo M, Hermoso JA, Håvarstein LS. 2020. Class A PBPs have a distinct and unique role in the construction of the pneumococcal cell wall. Proc Natl Acad Sci U S A 117:6129–6138. https://doi.org/10.1073/pnas.1917820117.
55. Su H-N, Li K, Zhao L-S, Yuan X-X, Zhang M-Y, Liu S-M, Chen X-L, Liu L-N, Zhang Y-Z. 2020. Structural visualization of septum formation in Staphylococcus warneri using atomic force microscopy. J Bacteriol 202:e00294-20. https://doi.org/10.1128/JB.00294-20.
56. Sambrook J, Russell DW. 2001. Molecular cloning: a laboratory manual. Cold Spring Harbor Laboratory Press, New York.
57. Gibson DG, Young L, Chuang R-Y, Venter JC, Hutchison CA, Smith HO. 2009. Enzymatic assembly of DNA molecules up to several hundred kilobases. Nat Methods 6:343–345. https://doi.org/10.1038/nmeth.1318.
58. Erster O, Liscovitch M. 2010. A modified inverse PCR procedure for insertion, deletion, or replacement of a DNA fragment in a target sequence and its application in the ligand interaction scan method for generation of ligand-regulated proteins. Methods Mol Biol 634:157–174. https://doi.org/10.1007/978-1-60761-652-8_12.

59. Schenk S, Laddaga RA. 1992. Improved method for electroporation of Staphylococcus aureus. FEMS Microbiol Lett 73:133–138. https://doi.org/10.1016/0378-1097(92)90596-g.
60. Novick RP, Morse SI. 1967. In vivo transmission of drug resistance factors between strains of Staphylococcus aureus. J Exp Med 125:45–59. https://doi.org/10.1084/jem.125.1.45.
61. García-Lara J, Weihs F, Ma X, Walker L, Chaudhuri RR, Kasturiarachchi J, Crossley H, Golestanian R, Foster SJ. 2015. Supramolecular structure in the membrane of Staphylococcus aureus. Proc Natl Acad Sci U S A 112:15725–15730. https://doi.org/10.1073/pnas.1509557112.
62. Zhao G, Meier TI, Kahl SD, Gee KR, Blaszczak LC. 1999. BOCILLIN FL, a sensitive and commercially available reagent for detection of penicillin-binding proteins. Antimicrob Agents Chemother 43:1124–1128. https://doi.org/10.1128/AAC.43.5.1124.
63. Zhou X, Halladin DK, Rojas ER, Koslover EF, Lee TK, Huang KC, Theriot JA. 2015. Mechanical crack propagation drives millisecond daughter cell separation in Staphylococcus aureus. Science 348:574–578. https://doi.org/10.1126/science.aaa1511.
64. Sutton JAF, Carnell OT, Lafage L, Gray J, Biboy J, Gibson JF, Pollitt EJG, Tazoll SC, Turnbull W, Hajdamowicz NH, Salamaga B, Pidwill GR, Condliffe AM, Renshaw SA, Vollmer W, Foster SJ. 2021. Staphylococcus aureus cell wall structure and dynamics during host-pathogen interaction. PLoS Pathog 17:e1009468. https://doi.org/10.1371/journal.ppat.1009468.
65. Hutter JL, Bechhoefer J. 1993. Calibration of atomic-force microscope tips. Rev of Scientific Instruments 64:1868–1873. https://doi.org/10.1063/1.1143970.
66. Sader JE, Borgani R, Gibson CT, Haviland DB, Higgins MJ, Kilpatrick JI, Lu J, Mulvaney P, Shearer CJ, Slattery AD, Thorén P-A, Tran J, Zhang H, Zhang H, Zheng T. 2016. A virtual instrument to standardise the calibration of atomic force microscope cantilevers. Rev Sci Instrum 87:093711. https://doi.org/10.1063/1.4962866.
67. Bertsche U, Kast T, Wolf B, Fraipont C, Aarsman MEG, Kannenberg K, von Rechenberg M, Nguyen-Distèche M, den Blaauwen T, Höltje J-V, Vollmer W. 2006. Interaction between two murein (peptidoglycan) synthases, PBP3 and PBP1B, in Escherichia coli. Mol Microbiol 61:675–690. https://doi.org/10.1111/j.1365-2958.2006.05280.x.
68. Kabsch W. 2010. XDS. Acta Crystallogr D Biol Crystallogr 66:125–132. https://doi.org/10.1107/S0907444909047337.
69. Evans PR, Murshudov GN. 2013. How good are my data and what is the resolution? Acta Crystallogr D Biol Crystallogr 69:1204–1214. https://doi.org/10.1107/S0907444913000061.
70. Winn MD, Ballard CC, Cowtan KD, Dodson EJ, Emsley P, Evans PR, Keegan RM, Krissinel EB, Leslie AGW, McCoy A, McNicholas SJ, Murshudov GN, Pannu NS, Potterton EA, Powell HR, Read RJ, Vagin A, Wilson KS. 2011. Overview of the CCP4 suite and current developments. Acta Crystallogr D Biol Crystallogr 67:235–242. https://doi.org/10.1107/S0907444910045749.
71. Bunkóczi G, Read RJ. 2011. Improvement of molecular-replacement models with Sculptor. Acta Crystallogr D Biol Crystallogr 67:303–312. https://doi.org/10.1107/S0907444910051218.
72. McCoy AJ, Grosse-Kunstleve RW, Adams PD, Winn MD, Storoni LC, Read RJ. 2007. Phaser crystallographic software. J Appl Crystallogr 40:658–674. https://doi.org/10.1107/S0021889807021206.
73. Emsley P, Lohkamp B, Scott WG, Cowtan K. 2010. Features and development of Coot. Acta Crystallogr D Biol Crystallogr 66:486–501. https://doi.org/10.1107/S0907444910007493.
74. Liebschner D, Afonine PV, Baker ML, Bunkóczi G, Chen VB, Croll TI, Hintze B, Hung LW, Jain S, McCoy AJ, Moriarty NW, Oeffner RD, Poon BK, Prisant MG, Read RJ, Richardson JS, Richardson DC, Sammito MD, Sobolev OV, Stockwell DH, Terwilliger TC, Urzhumtsev AG, Videau LL, Williams CJ, Adams PD. 2019. Macromolecular structure determination using X-rays, neutrons and electrons: recent developments in Phenix. Acta Crystallogr D Struct Biol 75:861–877. https://doi.org/10.1107/S2059798319011471.
75. Chen VB, Arendall WB, Headd JJ, Keedy DA, Immormino RM, Kapral GJ, Murray LW, Richardson JS, Richardson DC. 2010. MolProbity: all-atom structure validation for macromolecular crystallography. Acta Crystallogr D Biol Crystallogr 66:12–21. https://doi.org/10.1107/S0907444909042073.
76. Krissinel E, Henrick K. 2007. Inference of macromolecular assemblies from crystalline state. J Mol Biol 372:774–797. https://doi.org/10.1016/j.jmb.2007.05.022.